

A NEAR-INFRARED SPECTROSCOPIC SURVEY OF 886 NEARBY M DWARFS

RYAN C. TERRIEN^{1,2,3,4}, SUVRATH MAHADEVAN^{1,2,3}, ROHIT DESHPANDE^{1,2}, CHAD F. BENDER^{1,2}

ApJS Accepted, August 2015

ABSTRACT

We present a catalog of near-infrared (NIR) spectra and associated measurements for 886 nearby M dwarfs. The spectra were obtained with the NASA-Infrared Telescope Facility SpeX Spectrograph during a two-year observing campaign; they have high signal-to-noise ratios (SNR > 100 – 150), span 0.8–2.4 μm and have $R \sim 2000$. Our catalog of measured values contains useful T_{eff} and composition-sensitive features, empirical stellar parameter measurements, and kinematic, photometric, and astrometric properties compiled from the literature. We focus on measures of M dwarf abundances ([Fe/H] and [M/H]), capitalizing on the precision of recently published empirical NIR spectroscopic calibrations. We explore systematic differences between different abundance calibrations, and to other similar M dwarf catalogs. We confirm that the M dwarf abundances we measure show the expected inverse dependence with kinematic, activity, and color-based age indicators. Finally, we provide updated [Fe/H] and [M/H] for 16 M dwarf planet hosts. This catalog represents the largest published compilation of NIR spectra and associated parameters for M dwarfs. It provides a rich and uniform resource for the nearby M dwarfs, and will be especially valuable for measuring Habitable Zone locations and comparative abundances of the M dwarf planet hosts that will be uncovered by upcoming exoplanet surveys.

Subject headings: stars: low-mass—stars: fundamental parameters—techniques: spectroscopic—stars: abundances

1. INTRODUCTION AND BACKGROUND

Recent years have seen a crescendo of observational and theoretical interest in the population of nearby M dwarfs. These stars, which make up the majority of the stars in the solar neighborhood (e.g. Reid et al. 2002), have historically been difficult to observe due to their optical faintness. During the past two decades, great strides have been made in the refinement of techniques for identifying nearby M dwarfs. Multiple groups have used parallaxes (e.g. Henry et al. 2006; Winters et al. 2011; Jao et al. 2011; Riedel et al. 2014), photometry, and proper motions to identify thousands of M dwarfs in the Solar neighborhood (Lépine & Shara 2005; Lépine & Gaidos 2011; Lépine et al. 2013; Frith et al. 2013; Gaidos et al. 2014) and throughout the Galaxy (West et al. 2011; Deshpande et al. 2013).

In parallel, tools for observationally characterizing these stars have improved dramatically (Reid et al. 1995; Hawley et al. 1996; Gizis et al. 2002; Reid et al. 2002; Lépine et al. 2007). Even so, the precise measurement of their stellar parameters remains challenging. Precise stellar radii and masses have only been measured for a small set of targets through interferometry (e.g. Demory et al. 2009; Boyajian et al. 2012) and the study of eclipsing binaries (e.g. Morales et al. 2009;

Carter et al. 2011). The measurement of M dwarf stellar compositions has also presented a formidable challenge, as the molecular species in their atmospheres mask the continuum (Gustafsson 1989), typically rendering the direct spectroscopic modeling techniques intractable (although progress is being made, e.g. Önehag et al. (2012)). Instead of direct modeling, the detailed analysis of atomic line and molecular absorption in M dwarf spectra has also been demonstrated (Woolf & Wallerstein 2005, 2006; Woolf et al. 2009).

Rather than depending solely on the M dwarf spectra to derive abundance information, several groups have instead relied on abundance measurements of associated stars. These calibrator systems typically contain an FGK dwarf in a common-proper-motion system with an M dwarf, separated by several arcseconds or more. The composition of the higher-mass star is known or readily determined using established spectroscopic techniques (as deployed for M subdwarfs in Gizis 1997). The M dwarf is then assumed to have the same composition, and their photometric and spectroscopic properties are used to construct empirical models that can then be applied to single stars. This empirical calibration strategy was first implemented for optical photometry ($V - K_s$, Bonfils et al. 2005), taking advantage of the strong and weak [Fe/H] dependence for M dwarf V and K_s -band absorption, respectively (Chabrier et al. 2000; Delfosse et al. 2000; Bonfils et al. 2005). Multiple groups have developed similar photometric calibrations based on absolute stellar magnitudes (Johnson & Apps 2009; Schlafman & Laughlin 2010; Neves et al. 2012; Johnson et al. 2012) and colors (Newton et al. 2014; Hejazi et al. 2015), and Neves et al. (2013a, 2014) have further leveraged these photometric [Fe/H] calibrations into more precise optical spectroscopic calibrations.

rct151@psu.edu

¹Department of Astronomy and Astrophysics, The Pennsylvania State University, 525 Davey Laboratory, University Park, PA 16802, USA.

²Center for Exoplanets and Habitable Worlds, The Pennsylvania State University, University Park, PA 16802, USA.

³The Penn State Astrobiology Research Center, The Pennsylvania State University, University Park, PA 16802, USA.

⁴Visiting Astronomer at the Infrared Telescope Facility, which is operated by the University of Hawaii under contract NNH14CK55B with the National Aeronautics and Space Administration.

This empirical calibration technique has also been implemented for near-infrared (NIR) spectra, taking advantage of the relative brightness of M dwarfs in the NIR. The first of these was the K_s -band calibration developed by Rojas-Ayala et al. (2010), which leveraged the K_s -band Na I doublet and Ca I triplet, along with H₂O absorption indices to account for T_{eff} effects. This technique was expanded by Terrien et al. (2012b, , T12), refined in Rojas-Ayala et al. (2012) and Newton et al. (2014) (hereafter N14), and further generalized in Mann et al. (2013a) (hereafter M13a). Presently, the NIR calibration with the largest number and diversity of calibrators is that of M13a for early-mid M dwarfs, and Mann et al. (2014) (hereafter M14) for late-type M dwarfs; these calibrations provide [Fe/H] and [M/H], are well-calibrated across a wide range of [Fe/H] ($-0.8 < [\text{Fe}/\text{H}] < 0.5$) and spectral type (late K to M8), and have good precision (~ 0.10 dex in [Fe/H] and [M/H]).

In addition to the empirical techniques for measuring stellar composition, various groups have developed similar techniques for the measurement of spectral type, effective temperature, stellar mass, and stellar radius, based on spectral type standards, stars with interferometrically-determined parameters, or stars with parameters measured through other means. Notably, techniques applicable to high resolution optical spectra from HARPS (Neves et al. 2013a, 2014; Maldonado et al. 2015) and Keck (Pineda et al. 2013) have achieved good precision for the M dwarfs observed in these programs. Techniques based on lower-resolution ($R \sim 2000$) NIR spectra, using T_{eff}-sensitive indices (Mann et al. 2013b) (hereafter M13b) and atomic absorption features (Newton et al. 2015) have been also been developed. The use of broadband photometry has also enabled precise measurements of the temperatures and radii of these stars (Mann et al. 2015). The resulting suite of techniques has been used extensively in the characterization of *Kepler* low-mass planet hosts (Muirhead et al. 2012a,b; Johnson et al. 2012; Ballard et al. 2013; Muirhead et al. 2013, 2014; Newton et al. 2015).

The tools and data described above, combined with advances in structural (Baraffe et al. 1998; Dotter et al. 2007; Spada et al. 2013) and atmospheric (Allard et al. 2012) models, provide a fertile ground for a variety of topics related to M dwarfs, including Galactic evolution (e.g. Bochanski et al. 2010, 2011), stellar structure (e.g. Lopez-Morales 2007; Reiners et al. 2012; Feiden & Chaboyer 2012; Torres 2013), and exoplanets. Nearby M dwarfs are appealing targets for Doppler Radial Velocity (RV) and transit exoplanet searches because their low masses and luminosities make planets orbiting in their Habitable Zones (HZ Kasting 1993; Kopparapu et al. 2013, 2014) more easily detectable than those around higher-mass stars. Moreover, given the prevalence of M dwarfs, their planets may represent the most common exoplanetary environment in the Galaxy. Upcoming NIR ground-based RV surveys such as the Habitable-zone Planet Finder on the Hobby-Eberly Telescope (HPF, Mahadevan et al. 2012), CARMENES (Quirrenbach et al. 2012) at Calar Alto, SPIrou on the CFHT (Thibault et al. 2012), IRD on Subaru (Kotani et al. 2014), and iLocater

on LBT as well as photometric surveys like TESS (Ricker et al. 2015), PLATO (Rauer et al. 2014), and MEarth (Nutzman & Charbonneau 2008) will specifically target planets around nearby M dwarfs. These surveys will provide unprecedented sensitivity to planets orbiting the nearby M dwarfs, whose optical faintness has made them difficult targets for many existing RV and transit surveys. Despite being optimized for optically bright FGK stars, results from *Kepler* (Borucki et al. 2010) clearly indicate that M dwarfs host a large population of small planets in the HZ (Dressing & Charbonneau 2015). The characteristics of planets around M dwarfs will be useful for testing theories of planet formation (e.g. Laughlin et al. 2004) in the regime of low stellar and protoplanetary disk masses.

In order to construct a well-characterized target list for HPF, we have carried out an extensive spectroscopic survey of 886 nearby M dwarfs, using the SpeX spectrograph at the NASA Infrared Telescope Facility (IRTF). We take advantage of the NIR spectroscopic techniques described above to measure the metallicities of these stars, in order to form the largest catalog yet of nearby M dwarf compositions based on spectroscopy. We also provide measurements of the T_{eff}-sensitive indices, which can be used to estimate stellar mass, radius, or luminosity. This work echoes the spirit of previous large-scale efforts to characterize our most common stellar neighbors (e.g. Reid et al. 1995; Riaz et al. 2006; Deshpande et al. 2013, N14).

In Section 2 we describe our observations and data reduction, including target selection and cross-identification with other catalogs. In Section 3 we describe our spectral measurements and error estimates. In Section 5 we provide a brief summary and discussion of our measurements and comparisons to other catalogs.

1.1. Published Results from this Sample

This dataset has already enabled a variety of studies of the nearby M dwarfs. T12 developed a new H -band [Fe/H] calibration for M dwarfs, extending established techniques (Bonfils et al. 2005; Woolf & Wallerstein 2006; Rojas-Ayala et al. 2010) and providing a valuable comparison for the development of improved calibrations (M13a) and a starting point for work with higher resolution spectra (e.g. SDSS-III APOGEE or IGRINS, Deshpande et al. 2013; Park et al. 2014). Terrien et al. (2012a) employed the T12 [Fe/H] measurement technique to characterize the low-mass eclipsing binary CM Draconis (CM Dra Morales et al. 2009), helping to remove the [Fe/H]-related degeneracy and to clarify the disagreement between models and observations of this system. Terrien et al. (2014) again applied the T12 [Fe/H] measurement technique to confirm the first low-mass members of the nearby Coma Berenices cluster (Trumpler 1938). Finally, Terrien et al. (2015) leveraged M dwarf activity catalogs (e.g. Gizis et al. 2002; Riaz et al. 2006; Gaidos et al. 2014) and improvements in parallax measurements of the nearby M dwarfs (e.g. Dittmann et al. 2014, and the Research Consortium on Nearby Stars, RECONS⁵) to develop new spectroscopic indices for M dwarf luminosity, surface gravity, and possibly α -enrichment.

⁵ <http://www.recons.org>

2. OBSERVATIONS AND DATA REDUCTION

Over a period of two years, beginning in 2011 May and concluding in 2013 August, we observed 886 M dwarfs with the SpeX NIR spectrograph on the NASA-IRTF (Rayner et al. 2003). This set of observations includes 21 stars observed multiple times.

2.1. Target Selection

We drew M dwarf targets primarily from the Lépine & Shara (2005, LSPM-N) and Lépine & Gaidos (2011, LG11) proper-motion based catalogs of nearby M dwarfs, and from published lists of M dwarf planet hosts⁶ and known wide binaries (drawn from Rojas-Ayala et al. 2010) that serve as abundance calibration stars. The majority of target stars (829) were taken from LG11, the remainder being the aforementioned binary calibrator stars, planet hosts, or that were targeted in a contemporaneous high-resolution survey (Deshpande et al. 2013). For stars from LG11 and LSPM-N, we prioritized targets with redder optical-to-infrared color ($V - J > 4$), a good indication of mid-late M spectral subtype (M4 or later). The resulting compilation of targets included both high-priority targets (calibrator stars, planet hosts, late-type M dwarfs) and low-priority targets (early type M dwarfs).

From this super-set of potential targets we constructed our nightly observing plans, and during each night we actively added and removed targets to account for changes in observing conditions. Our primary goal was to ensure very high signal-to-noise ($\text{SNR} > 200$ per pixel) for high-priority targets, and our secondary goal was to observe as many M dwarfs as possible with reasonable SNR (> 100). The typical resulting observing pattern was a series of groups (in position and time) which contained a few faint late-type (M4 or later) M dwarfs and several brighter early (earlier than M4) M dwarfs. Each group was sufficiently localized that a single nearby standard star (within one hour of time and 0.1 sec z of target star) could be used for telluric correction, and the same arc lamp exposure could be used for wavelength calibration. This strategy enabled a large number of M dwarfs to be observed, with minimal time losses from large slews, wavelength calibrations, and standard star observations.

2.2. Data Reduction

We obtained uniform data for all observations, operating SpeX in the short cross-dispersed (SXD) mode with the $0.3 \times 5''$ slit, which produces $R \sim 2000$ spectra from 0.8 - 2.4 μm . As described in T12, we extracted these spectra with the facility-provided SpeXTool package (Cushing et al. 2004). We telluric-corrected using the `xtellcor` program (Vacca et al. 2003) and observations of an A0V star (or similar), at an airmass and observation time within 0.1 (sec z) and 1 hour of the target, respectively. The `xtellcor` program also flux-calibrates the spectrum, using the optical magnitudes (from SIMBAD) of the standard star to estimate its flux as a function of wavelength. Vacca et al. (2003) estimate that the flux calibration using this method agrees to within a few percent of fluxes derived using broadband magnitudes.

⁶ e.g. <http://exoplanets.org>

A typical example spectrum is shown in Figure 1. All observations presented here took place prior to the SpeX detector upgrade, which occurred in the spring of 2014.

2.3. Cross-Identification with other catalogs

We cross-identified our targets with several published catalogs, in order to provide supplementary data for our target stars and to facilitate the use of our catalog. Each target has a 2MASS (Skrutskie et al. 2006) identifier, and we use the 2MASS J2000 coordinates in our final catalog. The 2MASS ID also provides the most convenient uniform identifier for all our targets. We include in our catalog the 2MASS J, H, K_s photometry and the respective quality flags for each star.

We cross-identified our targets with the UCAC4 (Zacharias et al. 2013) catalog as well. UCAC4 provides optical magnitudes based on the AAVSO Photometric All-Sky Survey (APASS). Optical magnitudes are useful for M dwarfs as their optical-to-infrared colors are excellent indicators of spectral type and T_{eff} ; we include UCAC4 aperture (A)-magnitudes (for 874 stars) and V -magnitudes (for 732 stars) as indications of their optical brightness.

For the majority of our targets, we include proper motions as measured by LG11 or LSPM-N. For targets without proper motions in these catalogs, we include measurements from UCAC4 or the PPMXL catalog (Roeser et al. 2010).

We also provide parallax measurements for a nearly half of our targets (427). Many of these parallax measurements are drawn from the RECONS database (Jao et al. 2005; Riedel et al. 2014, 2010; Henry et al. 2006) and the newly-published MEarth parallax catalog (Dittmann et al. 2014). We also found parallaxes in several other catalogs (van Altena et al. 1995; van Leeuwen 2007; Gould & Chaname 2004; Anglada-Escudé et al. 2012; Harrington et al. 1993; Gatewood 2008; Monet et al. 1992; Lépine et al. 2009).

3. SPECTRAL MEASUREMENTS

We describe here the various spectral measurements we performed on the M dwarf spectra.

3.1. Band Indices and Spectral Type

The NIR spectra of M dwarfs are dominated by the broad absorption of H_2O , the strength of which is known to correlate strongly with T_{eff} and spectral type (e.g. Wilking et al. 1999). Using $R \sim 2000$ NIR spectra like ours, several groups have developed H_2O -based and other indices that are well-correlated with spectral type and T_{eff} (Covey et al. 2010; Rojas-Ayala et al. 2010, 2012, T12, M13a, M13b, N14, M14). Calibrations of these indices provide an efficient and simple method for measuring spectral type and temperature for the M dwarfs in our catalog. The relatively large widths of the wavelength ranges used in these measurements makes them insensitive to small errors in the RV measurement. For the M dwarfs in our catalog, we measured the T_{eff} -sensitive indices used in M13b and N14 (Covey et al. 2010; Rojas-Ayala et al. 2012; Mann et al. 2013a) (see Table 1).

To measure spectral type for the M dwarfs in our catalog, we applied the NIR calibration developed in

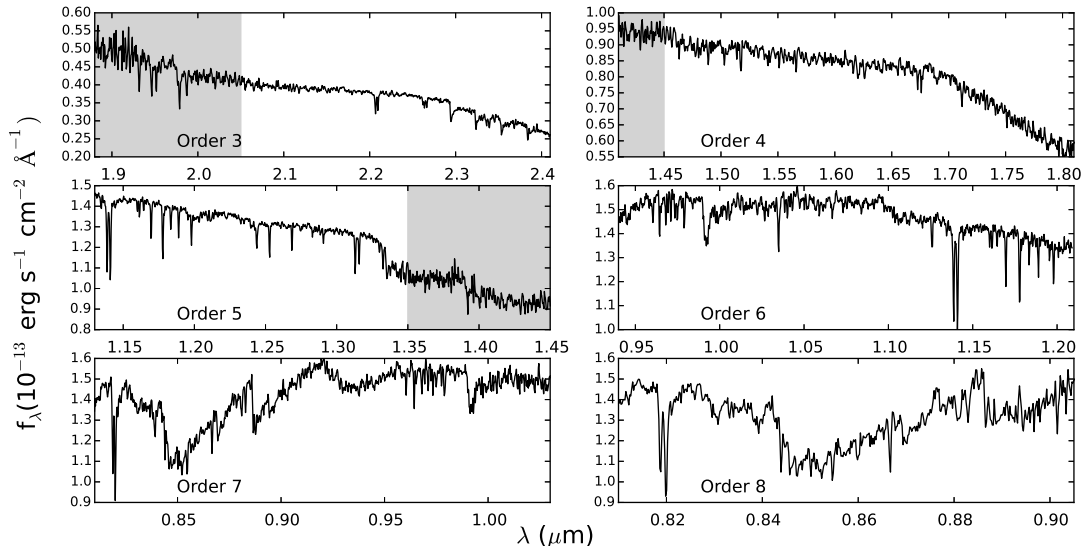


Figure 1. The six separate telluric-corrected orders of the IRTF-SpeX SXD spectrum of GJ 1103A, which is a typical M4.5V star from our survey. Regions with significant telluric contamination are shaded in gray.

Table 1
Parameters of T_{eff} -Sensitive Indices^a

Name	Range 1 (Å)	Range 2 (Å)	Range 3 (Å)
Mann et al. (2013b) <i>J</i> Index	10087.5 – 10172.5	10967.5 – 11052.5	11587.5 – 11672.5
Mann et al. (2013b) <i>H</i> Index	14625.0 – 14655.0	16615.0 – 16645.0	17945.0 – 17975.0
Mann et al. (2013b) <i>K</i> Index	20242.5 – 20277.5	22747.5 – 22782.5	23367.5 – 23402.5
Mann et al. (2014) $\text{H}_2\text{O}-J$	12100.0 – 12300.0	13130.0 – 13330.0	13310.0 – 13510.0
Covey et al. (2010) $\text{H}_2\text{O}-H$	15950.0 – 16150.0	16800.0 – 17000.0	17600.0 – 17800.0
Rojas-Ayala et al. (2012) $\text{H}_2\text{O}-K$	20700.0 – 20900.0	22350.0 – 22550.0	23600.0 – 23800.0

^a Value of index = $(\langle F_1 \rangle - \langle F_2 \rangle) / (\langle F_2 \rangle - \langle F_3 \rangle)$

N14, which is based on the $\text{H}_2\text{O}-K2$ index developed in Rojas-Ayala et al. (2012). This calibration yields “NIR M sub-types” on a uniform scale for our stars. The precise relationship between this NIR M sub-type and the established Palomar/Michigan State University (PMSU) scale (Reid et al. 1995; Hawley et al. 1996) is considered in Rojas-Ayala et al. (2012) and N14, and is known to be sensitive to $[\text{Fe}/\text{H}]$ for at least the early M dwarfs. We also include in our catalog the measured PMSU spectral types from the N14 PMSU spectral type calibration over the range in which it is valid (M1-M4).

To check the consistency of our NIR spectral type measurements, we considered the overlap between our sample and that of N14, which includes 152 M dwarfs. We found no significant offset between the respective measures of spectral type, and a scatter of half a subtype, consistent with the scatter expected from N14.

This NIR spectral type measurement was necessarily the first in our chain of measurements, as it defined the template for our measurement of RV. The T_{eff} -sensitive features are sufficiently broad that they are insensitive to RV shifts in our $R \sim 2000$ spectra. Nonetheless, after measuring the RV we re-measured the spectral type in the rest frame of the star, and this is the value we report in our catalog.

3.2. Radial Velocity

We measured the RV of each order of each spectrum by fitting a Gaussian to the cross-correlation (in $\log-\lambda$) of the observed spectrum with a spectral template of similar spectral type. We used three spectral templates from the IRTF Cool Stars Library (Cushing et al. 2005; Rayner et al. 2009): for stars M4 and earlier we used the M1.5V star HD 36395, for stars M5 to M6 we used the M5V star G1 51, and for stars later than M6 we used the M9V star LHS 2065. For each observation, we report the weighted (by SNR) average RV from all orders, and this is value we used to shift all spectra to a common frame for further analysis.

To verify our RV measurements, we compared our (barycentric-corrected) RV measurements to those measured in Chubak et al. (2012) and N14. For the 33 stars in common with (Chubak et al. 2012), we find a median offset of $+7.6 \text{ km s}^{-1}$ with a standard deviation of 8.7 km s^{-1} . For 152 stars in common with N14, we find a median offset of $+7.9 \text{ km s}^{-1}$ with a standard deviation of 13.2 km s^{-1} . Figure 2 shows the differences in RV between this work and the literature sources. Among our common targets with the N14 study, there were seven with differences greater than 40 km s^{-1} . Two of these (2MASS J07362513+0704431/GJ 3454 and 2MASS J17074083+0722066/GJ 1210) are known visual binaries with sub-arcsecond separation (Pravdo et al. 2005; Janson et al. 2014). Given the consistency of the RV measurements of the majority of the common targets,

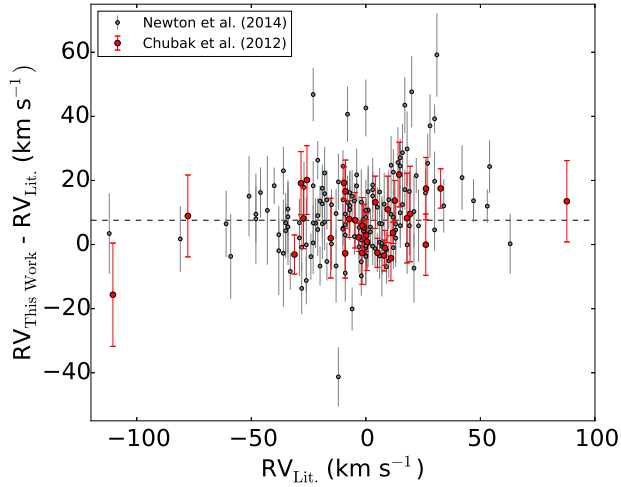


Figure 2. Differences between the RVs measured in this work and those measured in Chubak et al. (2012) and N14. The median differences are shown as dashed lines, and are both approximately 8 km s^{-1} .

we suspect that these highly discrepant targets are either RV-variable or binary stars. We also measure a large RV for one star (2MASS J06052936+6049231/LHS 1817, -113.9 km s^{-1}) with similar magnitude but the opposite sign as N14 and Shkolnik et al. (2012).

That the systematic offset from N14 and Chubak et al. (2012) would be similar is unsurprising, as N14 implement a $\sim 2.6 \text{ km s}^{-1}$ correction to match the RV system of Chubak et al. (2012). The origin of the $\sim 7-8 \text{ km s}^{-1}$ offset for our data is unclear; since we rely solely on the arc lamp wavelength calibrations, we are subject to different and possibly worse instrumental systematics than N14, who use telluric spectra to refine their wavelength calibrations. A systematic issue with the wavelength calibration of approximately 8 km s^{-1} is also supported by the magnitudes of the inter-order and RV template differences, as discussed in Section 3.6.

In order to obtain barycentric RVs in the same system as (Chubak et al. 2012) and N14, the median offset above ($\sim 7.6 \text{ km s}^{-1}$) should be added to the RVs in our catalog.

3.3. Effective Temperature and Related Parameters

Due to the difficulty of modeling M dwarf atmospheres and spectra, model-dependent measurements of T_{eff} can systematically differ by 100 K or more (Rajpurohit et al. 2013, and references therein). Interferometric T_{eff} measurements have therefore been crucial in defining the M dwarf T_{eff} scale, and in parsing the relations between the fundamental parameters of M dwarfs (Boyajian et al. 2012, and references therein). However, there are few targets with spectral type M5 or later that are bright enough or have large enough angular diameters to support precise interferometric radius measurements. To enable stellar radius measurements without interferometry, multiple groups have constructed empirical calibrations based on photometry (Boyajian et al. 2012), spectral indices (M13b), or individual absorption feature strengths (Newton et al. 2015).

We measured T_{eff} for the M dwarfs in our catalog using the H_2O indices as discussed in Section 3.1. We used the J, H, K_s T_{eff} calibrations developed in M13b over their

well-calibrated range (e.g. $1.0 < \text{H}_2\text{O}-K < 1.37$), which corresponds to $3300 < T_{\text{eff}} < 4800 \text{ K}$. M13b provide empirical relations for stellar radius, luminosity, and mass as a function of T_{eff} , calibrated on a set of stars with interferometrically measured parameters. We favor the use of the K_s -band index and calibrations due to the robustness of this index to small changes in the telluric correction (as discussed in Section 3.1).

We also measured T_{eff} , stellar radius, and stellar luminosity using the H -band atomic feature strengths studied in Newton et al. (2015). We measure the pseudo-equivalent widths (EWs) of these features using the continuum and feature definitions in their Table 1. They construct relations using the strengths and ratios of Mg and Al lines in M dwarfs, empirically calibrated on stars with interferometrically measured parameters. These relations use a similar calibration set to that of M13b, so the range of validity is similar: $3200 < T_{\text{eff}} < 4800 \text{ K}$.

3.4. Composition

We measured $[\text{Fe}/\text{H}]$ and $[\text{M}/\text{H}]$ using the empirical spectroscopic calibrations from T12, M13a, M14, and N14. These calibrations were all developed using data from the same spectrograph (IRTF-SpeX) in the same settings (SXD) as ours, so their recipes can be applied directly to our data. M13a present separate calibrations for features in the J, H, K_s bands that yield both $[\text{Fe}/\text{H}]$ and $[\text{M}/\text{H}]$ for early-mid M dwarfs (M1-M5). They derived these calibrations from a blind search of the most $[\text{Fe}/\text{H}]$ and $[\text{M}/\text{H}]$ -sensitive regions of the spectra in 112 stars with known $[\text{Fe}/\text{H}]$ and $[\text{M}/\text{H}]$, and are based on the EWs of a small number (four or fewer) of spectral regions in each case. The calibrations are valid for K5-M5 dwarfs and over approximately $-1.0 < [\text{Fe}/\text{H}] < +0.56$. We report the results of these calibrations separately for each target in our catalog.

For a similar range of targets in spectral type and $[\text{Fe}/\text{H}]$, we also report the K_s -band $[\text{Fe}/\text{H}]$ calibration developed in N14, which depends only on the EW of the K_s -band Na I doublet. N14 calibrated this relation using 36 M dwarfs with known $[\text{Fe}/\text{H}]$, and it is similar in form to the relations developed in (Rojas-Ayala et al. 2010) and (Rojas-Ayala et al. 2012). It is valid for M1-M5 dwarfs and for a range of $-1.00 < [\text{Fe}/\text{H}] < +0.35$.

For the late M dwarfs (M5 or later), the only applicable published $[\text{Fe}/\text{H}]$ calibration is that of (M14). The M14 calibration is based on two strong features in the K_s -band, the Ca I triplet and the Na I doublet, which were also used in the calibration of Rojas-Ayala et al. (2010) and Rojas-Ayala et al. (2012) for early-type M dwarfs. This calibration is based on 44 M dwarfs with known metallicities. It is an extension of the binary calibration technique described above, which extends the calibration set by including some early+late M dwarf pairs where the earlier-type M dwarf $[\text{Fe}/\text{H}]$ has itself been measured using empirical calibrations. This late-type calibration is valid for M4.5-M9.5 dwarfs and for a range of $-0.58 < [\text{Fe}/\text{H}] < +0.56$. The summary of the parameters of this $[\text{Fe}/\text{H}]$ calibration and those above is shown in Table 2.

For general comparison with other catalogs, and for cases below in which it is useful to have a single $[\text{Fe}/\text{H}]$ measurement for a given star, we elect to use the K_s -band calibrations of M13a for M1-M5 (see Section 5.3), along

with the output of M14 for M5 and later. We also report the $[M/H]$ values where available. For the purposes of presenting and vetting our catalog, we primarily consider $[Fe/H]$ as this is the specific quantity addressed by the bulk of work on the topic of M dwarf compositions.

3.5. Activity and gravity-sensitive lines

Our spectra extend to approximately $0.8 \mu\text{m}$ on the blue end, and so contain the 8200\AA Na I doublet (hereafter Na I) and the 8600\AA Ca II triplet (hereafter Ca II), strong features that have shown promise as indicators of activity (e.g. Kafka & Honeycutt 2006; Barnes et al. 2014) and surface gravity (Schlieder et al. 2012). Our measurements of these features for a subset of the observed M dwarfs showed a strong relationship with the T_{eff} and $[Fe/H]$ measures in these stars, and can be used to derive information about their radii, luminosities, and possibly α -enrichment. These measurements are discussed in (Terrien et al. 2015); we repeat the salient details here.

We measured the EWs of the Na I and Ca II features (EW_{NaI} , EW_{CaII}) for each of our targets. For Na I, we chose line and pseudo-continuum regions similar to those used in Martín et al. (2010), Schlieder et al. (2012), and Galvez-Ortiz et al. (2014). For Ca II, we defined feature regions for each of the three lines, as well as pseudo-continuum regions blueward and redward of each line. In each case, we fit a line to the pseudo-continuum regions in order to define the pseudo-continuum, and calculated the feature EW relative to this line. For EW_{NaI} and EW_{CaII} we follow the convention that positive EW corresponds to line absorption.

We caution that the Ca II and Na I features are embedded in regions of strong TiO and other absorption (as can be seen in e.g. Rayner et al. (2009)), so the EWs we measure are likely strongly sensitive to effects of the line species themselves as well as to the species that define the local pseudo-continuum. Moreover the SNR in the relevant orders of the SpeX spectra (orders seven and eight) is typically only a third of that in the J, H, K_s bands. Accordingly, these feature strengths should be carefully vetted before they are used in any application. The regions we defined for this analysis are listed in Table 3 and are shown on example spectra in Figure 3. Figure 3 also shows the three (possibly young) M dwarfs in our sample for which the Ca II lines are in emission.

3.6. Estimation of Uncertainties

In order to estimate our measurement uncertainties (for all quantities other than RV), we rely on a set of 21 M dwarfs with multiple observations. We calculate the RMS of the epoch-to-epoch differences in each measurement to obtain an observational estimate of our internal uncertainty. These values are shown for $[Fe/H]$, $[M/H]$, M spectral sub-type, Na I, and Ca II in Figure 4, for the T_{eff} -sensitive indices in 5, and for the H -band features of Newton et al. (2015) in Figure 6. For the Ca II and Na I features, we exclude three pairs with very low SNR (< 60). The observed RMS differences naturally include effects that arise from variable telluric conditions and by-hand choices in the telluric correction pipeline. The resultant variable quality of the telluric correction can induce correlated noise which dominates our errors at the high SNRs we achieve (N14).

We note that the T_{eff} -sensitive indices may be affected by the broad characteristics of the telluric correction, including the flux calibration (which uses SIMBAD B, V magnitudes, Section 2.2) and the construction of the telluric spectrum. By repeating the telluric correction with varying B, V magnitudes for a small set of stars, we found that the J -band indices were generally much more sensitive to differences in B, V magnitude and small differences in the by-hand components of the telluric correction. We favor the use of the K_s -band indices ($H_2O\text{-}K2$ or the M13b K_s -index), which are stable to a few percent or better with B, V variations of 0.5 mag.

The T_{eff} -sensitive indices can be used to estimate stellar T_{eff} (also mass and bolometric luminosity) as described in M13b, who present uncertainties of $70 - 100$ K for these relations. Our adopted measurement uncertainties for their T_{eff} -sensitive indices ($\sim 0.01 - 0.02$) correspond to median uncertainties of 110 K (J), 170 K (H), and 78 K (K_s) when propagated through the T_{eff} -index relations from M13b.

The H -band atomic feature strengths presented in Newton et al. (2015) can similarly be used in empirical calibrations to derive stellar T_{eff} (residual scatter = 73 K), luminosity ($0.049 L_{\odot}$), and radius ($0.027 R_{\odot}$). Our repeated measurements of these H -band features (Figure 6) suggests errors of $0.1 - 0.2 \text{\AA}$, which corresponds to measurement errors of approximately 90 K, $0.04 R_{\odot}$, and $0.07 \log L_{\odot}$.

To estimate the RV measurement uncertainty, we report the standard deviation of the RVs measured from each spectral order. This empirical measure of uncertainty is conveniently available for all targets, and avoids potential issues of RV variability which may occur using the epoch-to-epoch RMS differences. The median RV spread is $\sim 5.7 \text{ km s}^{-1}$. We note that a significant component of this RV spread is contributed by systematic offsets of $\sim 2 - 15 \text{ km s}^{-1}$ between spectral orders. We found these shifts to be variable depending on the choice of RV template spectrum, suggesting issues with the wavelength calibration, line shapes, or PSF changes. We also found overall RV differences of a similar magnitude ($\pm 20 \text{ km s}^{-1}$) for each star depending on the template used, suggesting that our RV precision is dominated by these systematic issues. This also suggests that the $\sim 7 \text{ km s}^{-1}$ offset between our RVs and those in the literature could be an artifact of the same systematic wavelength calibration issue.

Alternatively, it is possible to calculate measurement uncertainties based on the errors reported by the SpeX-Tool pipeline, which reports a combined noise that includes photon noise, read noise, and residual background noise components. Measurement uncertainties can then be estimated using Monte Carlo realizations of the noise. This process does not naturally include correlated noise effects like those arising from the telluric correction, although an ad-hoc technique is presented in N14 that mimics the effects of correlated noise. Briefly, this procedure involves convolving the noise “spectrum” with a 1.5 pixel gaussian, which is a good approximation for the actual autocorrelation function for observed spectra. This procedure effectively spreads the noise for each pixel over the neighboring pixels, mimicking the effect of the systematic correlated errors. Applying this technique to

Table 2
Parameters of primary empirical calibrations

Calibration	SpT Range	Metallicity Range	Error
Mann et al. (2013a) $[\text{Fe}/\text{H}]_K$	K5.0–M5.0	$-1.04 < [\text{Fe}/\text{H}] < +0.56$	0.11 dex
Mann et al. (2013a) $[\text{M}/\text{H}]_K$	K5.0–M5.0	$-0.70 < [\text{M}/\text{H}] < +0.50$	0.10 dex
Mann et al. (2014) $[\text{Fe}/\text{H}]_K$	M4.5–M9.5	$-0.58 < [\text{Fe}/\text{H}] < +0.56$	0.07 dex
Newton et al. (2014) $[\text{Fe}/\text{H}]$	M1.0–M5.0	$-1.00 < [\text{Fe}/\text{H}] < +0.35$	0.12 dex
Newton et al. (2014) NIR SpT	M1.0–M9.0	...	0.5 subtype

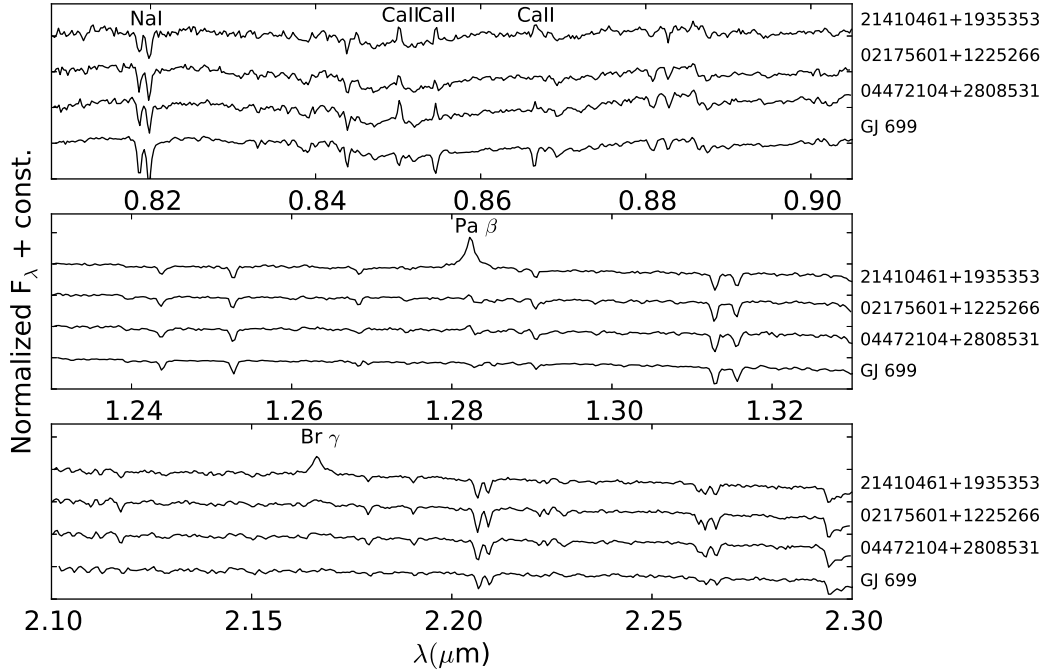


Figure 3. Three stars in the survey sample that have strong emission lines, along with GJ 699 as an example of a typical M dwarf. Three spectral regions with strong emission lines are shown: the top highlights the NIR Ca triplet, the middle highlights the H Pa β line, and the bottom highlights the H Br γ line. The top panel also identifies the Na I and Ca II features described in Section 3.5.

Table 3
Definitions for 8200Å Na I and 8600Å Ca II

Feature	Center (Å)	Width (Å)	PC Blue ^a (Å)	PC Red ^a (Å)
Na I	8192	34.0	8149 - 8169	8230 - 8270
Ca II ₁	8500	12	8456 - 8488	8512 - 8536
Ca II ₂	8544	12	8512 - 8536	8553 - 8573
Ca II ₃	8664	12	8635 - 8652	8672 - 8688

^a PC = Pseudo-continuum region definition.

our measurements yields error estimates that are consistently smaller than the observed epoch-to-epoch RMS differences, so we elect to report the more conservative RMS numbers as our estimated measurement uncertainties.

We note that the EW_{NaI} and EW_{CaII} are thought to be sensitive to chromospheric activity (Kafka & Honeycutt 2006; Barnes et al. 2014; Terrien et al. 2015), and may be variable on the timescales (days-months) of our repeated observations. The epoch-to-epoch RMS differences may therefore be an overestimate of our measurement error for these features. We also estimate a lower limit of ~ 0.1 Å on the measurement uncertainties for these features using

a 100-trial Monte Carlo technique based on the errors reported by the SpeXTool pipeline. Following N14, we include an ad hoc correction to account for the effects of correlated noise. The true measurement errors for Na I and Ca II likely lie in the range bracketed by these estimates, 0.1 – 0.5 Å.

4. CATALOG DESCRIPTION

We provide here a brief description of the spectra of the M dwarfs observed in this survey, as well as the set of measured and compiled values for each M dwarf.

4.1. The Spectra

The spectra for each of the 886 M dwarfs are available as a **gzipped** archive of standard FITS tables hosted at the Penn State Scholarsphere data hosting service⁷. The file for each spectrum is identified by the 2MASS ID of the target star. The FITS headers contain the standard information output by the SpeXTool pipeline, including observation meta-data (instrument configuration, airmass, observing time, etc.) and the SpeXTool-generated file history. We append to this the measured

⁷ <https://scholarsphere.psu.edu/files/5712mq85s#.VWNMS9rBzGc>

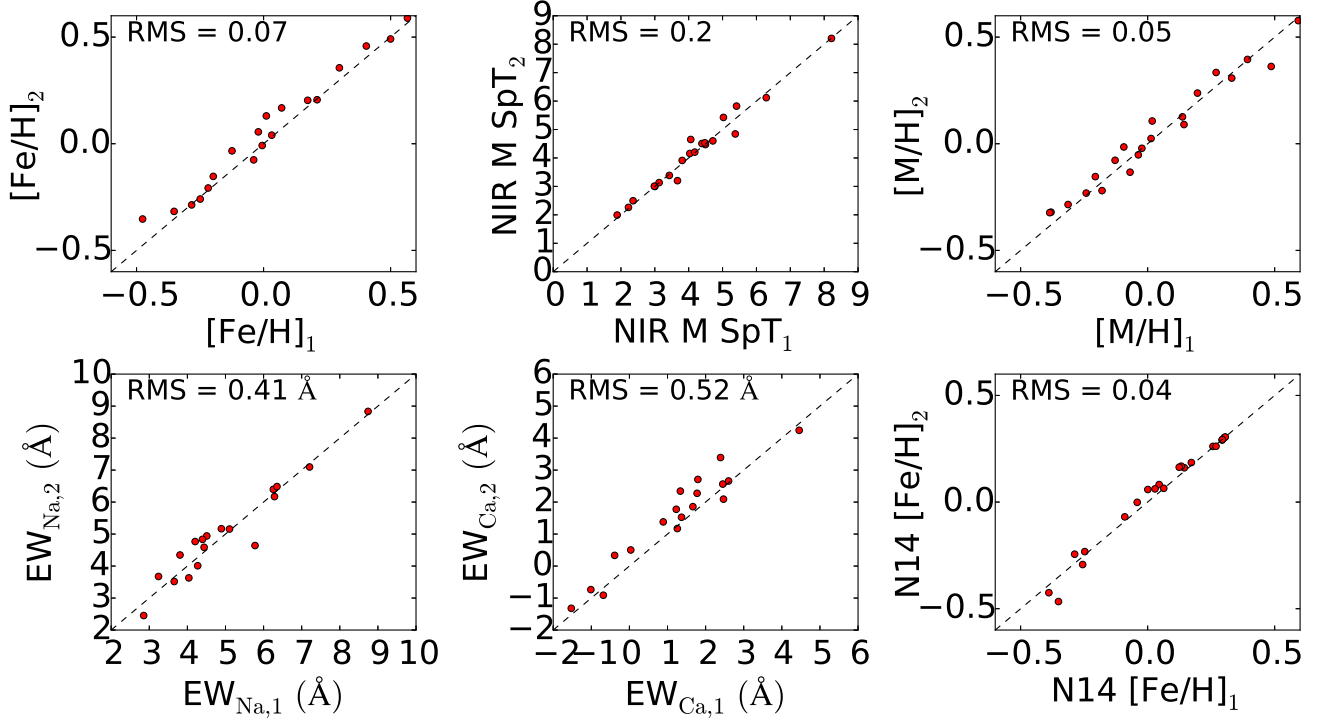


Figure 4. For targets we observed multiple times, the comparison of the $[\text{Fe}/\text{H}]$ (including our primary $[\text{Fe}/\text{H}]$ as discussed in Section 3.4 and using the technique of N14), $[\text{M}/\text{H}]$, M subtype, and Ca II and Na I feature strength measurements, from two different epochs. The black lines indicate a one-to-one relation. We adopt the observed RMS scatter in each case as our measurement uncertainty.

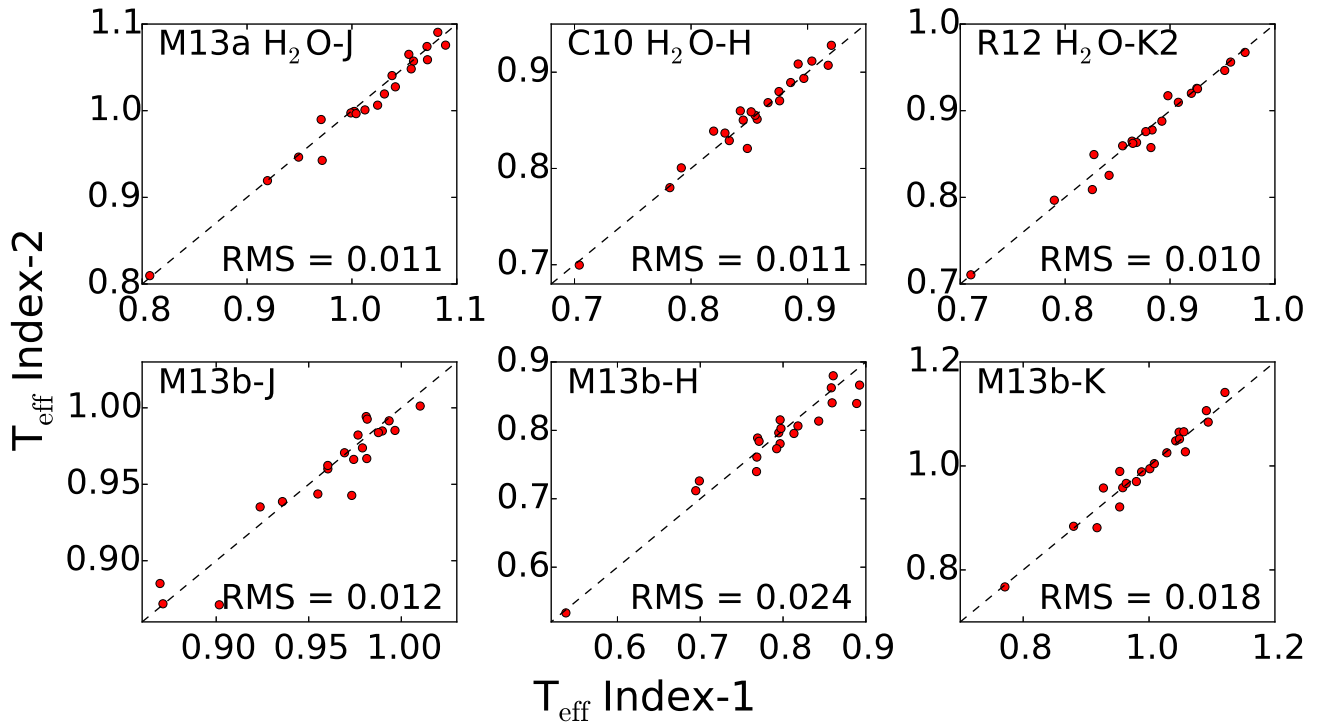


Figure 5. For targets we observed multiple times, the comparison of the T_{eff} -sensitive index measurements from two different epochs. N14 refers to the bands defined in N14, and M13 refers to those defined in M13b. The black lines indicate a one-to-one relation. We adopt the observed RMS scatter in each case as our measurement uncertainty.

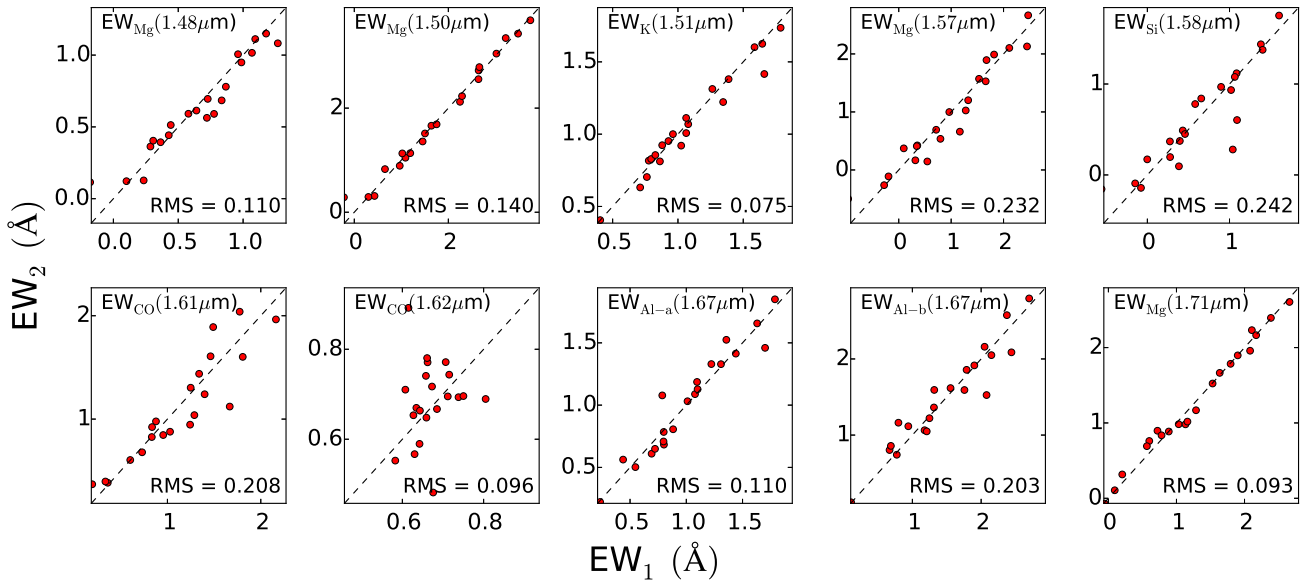


Figure 6. For targets we observed multiple times, the comparison of the Newton et al. (2015) feature strength measurements from two different epochs. The black lines indicate a one-to-one relation. We adopt the observed RMS scatter in each case as our measurement uncertainty.

RV shifts and barycentric correction for each spectrum, which can be used to velocity shift the spectra into a common reference frame.

The spectra themselves are in the standard format described fully in the SpeXTool documentation (Cushing et al. 2004)⁸. Briefly, each spectrum is a three-dimensional array, with the following axes:

1. Order number (3 – 8).
2. Data type (wavelength, flux, or variance). Wavelength is in vacuum, and is in the observer’s reference frame.
3. Pixel number.

4.2. The Catalog

Table 4 describes the columns included in our catalog. There is one line per star, including astrometry and photometry compiled from the literature, measurements of spectral features, and derived stellar parameters. The full machine-readable table is available in the online edition of The Astrophysical Journal Supplement.

5. GENERAL DISCUSSION

The overall distribution of our sample in NIR spectral type and $[\text{Fe}/\text{H}]$ is shown in Figure 7. The $[\text{Fe}/\text{H}]$ distribution of our sample is centered around solar, with a median $[\text{Fe}/\text{H}]$ of +0.05 dex and a scatter of 0.23 dex. This sample is neither volume nor magnitude-limited, but is consistent with the quoted $[\text{Fe}/\text{H}]$ measurement uncertainty (0.07 – 0.11 dex) and volume-limited measurements of the FGK stars (Casagrande et al. 2011) and M dwarfs (Johnson & Apps 2009) in the solar neighborhood, which find a median $[\text{Fe}/\text{H}]$ of ~ -0.05 dex and a scatter of ~ 0.2 dex. The distribution of NIR spectral types, which peaks around M4 and has a long tail toward earlier spectral types, is mostly a byproduct of our observational strategy, although the mass function of the Solar neighborhood also peaks around this spectral type (Henry et al. 2006).

5.1. Internal Comparisons

The majority of M dwarfs in our catalog have spectral types of M5 or earlier, and so can have their $[\text{Fe}/\text{H}]$ measured with multiple techniques. We focus on the most recent of these calibrations (from M13a and N14), along with the H -band calibration of T12 for comparison. Our measures of $[\text{Fe}/\text{H}]$ are compared to each other in Figure 8, which clearly shows systematic offsets among the various calibrations of up to 0.2 – 0.3 dex. In general, the H and J -band techniques are in agreement, while the K_s -band techniques show good agreement up to the saturation of the N14 calibration around 0.3 dex.

To explore whether issues with the wavelength calibration could be responsible for these systematic differences, we tested the sensitivity of the various $[\text{Fe}/\text{H}]$ calibrations to RV shifts. We measured $[\text{Fe}/\text{H}]$ for each target 50 times with a normal distribution of RVs centered around the original measured RV and with a spread equivalent to our estimated systematic and random measurement

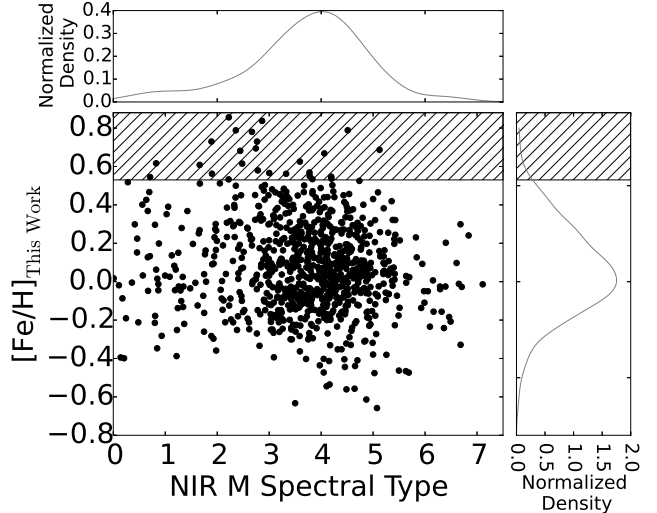


Figure 7. The spectral type and $[\text{Fe}/\text{H}]$ distributions for all M dwarfs observed in our survey. Our $[\text{Fe}/\text{H}]$ values are the average of the J , H , K_s -band calibrations from M13a for targets with spectral type M5 and earlier, and the $[\text{Fe}/\text{H}]$ derived from K_s band features using the technique from M14 for targets with spectral type later than M5. The hatched region shows $[\text{Fe}/\text{H}]$ values that exceed the calibrated range. The projection plots show a kernel density estimation for each parameter, clarifying the peaks, widths, and tails of each distribution.

errors (typically 10-20 km s^{-1}). Among the M13a calibrations, we found that the mean scatter in the K_s -band calibration was best (at ~ 0.02 dex), compared to the H -band (~ 0.03 dex) and J -band (~ 0.04 dex). This suggests that the features chosen for the M13a J and H -band calibrations are marginally more sensitive than the K_s -band features to small wavelength shifts, and the magnitude of the expected RV errors is not sufficient to explain the observed offsets. We found that an RV shift of $> 100 \text{ km s}^{-1}$ can remove the offset between the K_s and H -band measurements, although this causes the J -band measurements to diverge further. In any case, such a large shift is not justified given the agreement among our per-order RV measurements, those for different RV templates, and between our overall RV measurements and literature values.

The differences among our implementations of the M13a techniques may be due to undiagnosed issues with the wavelength calibration or other unidentified differences between our reduction procedure and those of M13a (e.g. the telluric correction). We present measurements from each band in our catalog, and justify below the choice of the K_s -band calibration of M13a as our preferred abundance calibration for M1-M5 dwarfs (Section 5.3).

5.2. Comparison to Other Catalogs

To check our results and to probe the relationships between different measures of metallicity, we compared our values (using the calibrations of M13a, M14, and N14) to those presented by a number of recent works (Rojas-Ayala et al. 2012; Gaidos et al. 2014, N14) for common targets. Rojas-Ayala et al. (2012) rely on the strengths of the K_s -band Na I and Ca I features along with the $\text{H}_2\text{O-K2}$ index to account of T_{eff} ; N14 rely on the strength of the K_s -band Na I feature alone;

⁸ Up-to-date manuals are available at the IRTF-SpeX website: <http://irtfweb.ifa.hawaii.edu/~spex/>

Table 4
M Dwarf Catalog Column Descriptions^a

Name	Description	Units
ID	2MASS Identifier	...
RADEG	Right Ascension in decimal degrees (J2000)	deg
DEDEG	Declination in decimal degrees (J2000)	deg
JMAG	2MASS <i>J</i> magnitude	mag
HMAG	2MASS <i>H</i> magnitude	mag
KSMAG	2MASS <i>K_s</i> magnitude	mag
E_JMAG	Error in 2MASS <i>J</i> magnitude	mag
E_HMAG	Error in 2MASS <i>H</i> magnitude	mag
E_KSMAG	Error in 2MASS <i>K_s</i> magnitude	mag
2MQF	2MASS quality flag	...
AMAG	UCAC4 <i>A</i> magnitude	mag
E_AMAG	Error in UCAC4 <i>A</i> magnitude	mag
PMRA	Proper motion in Right Ascension	mas/yr
PMDEC	Proper motion in Declination	mas/yr
R_PM	Reference for Proper Motion	...
PLX	Parallax	mas
E_PLX	Error in parallax	mas
R_PLX	Reference for parallax	...
VMAG	<i>V</i> magnitude from UCAC4	mag
RV	Radial Velocity	m/s
E_RV	Error in Radial Velocity (scatter among spectral orders)	m/s
BC	Barycentric Correction	m/s
MH2OJ	H ₂ O-J index defined by Mann et al. 2013a	...
CH2OH	H ₂ O-H index defined by Covey et al. 2010	...
RH2OK2	H ₂ O-K ₂ index defined by Rojas-Ayala et al. 2012	...
MJI	J index defined by Mann et al. 2013b	...
MHI	H index defined by Mann et al. 2013b	...
MKI	K index defined by Mann et al. 2013b	...
NSPT	M Spectral Subtype defined in Newton et al. 2014	...
NSPT_PMSU	PMSU Spectral Type defined in Newton et al. 2014	...
MTEFFJ	Effective Temperature from J index defined in Mann et al. 2013	K
MTEFFH	Effective Temperature from H index defined in Mann et al. 2013	K
MTEFFK	Effective Temperature from K index defined in Mann et al. 2013	K
MFEHJ	[Fe/H] from <i>J</i> -band defined in Mann et al. 2013	...
MFEHH	[Fe/H] from <i>H</i> -band defined in Mann et al. 2013	...
MFEHK	[Fe/H] from <i>K</i> -band defined in Mann et al. 2013	...
MMHJ	[M/H] from <i>J</i> -band defined in Mann et al. 2013	...
MMHH	[M/H] from <i>H</i> -band defined in Mann et al. 2013	...
MMHK	[M/H] from <i>K</i> -band defined in Mann et al. 2013	...
MFEHL	[Fe/H] for late-type M dwarfs defined in Mann et al. 2014	...
NFEH	[Fe/H] defined in Newton et al. 2014	...
T12FEHH	[Fe/H] from <i>H</i> -band defined in Terrien et al. 2012	...
EWNA	Equivalent Width of 820nm Na I doublet	0.1nm
EWCA	Equivalent Width of 860nm Ca II triplet	0.1nm
NMG148	Equivalent Width of 1.48 μ m Mg feature defined in Newton et al. 2015	0.1nm
NMG150	Equivalent Width of 1.50 μ m Mg feature defined in Newton et al. 2015	0.1nm
NK151	Equivalent Width of 1.51 μ m K feature defined in Newton et al. 2015	0.1nm
NMG157	Equivalent Width of 1.57 μ m Mg feature defined in Newton et al. 2015	0.1nm
NSI158	Equivalent Width of 1.58 μ m Si feature defined in Newton et al. 2015	0.1nm
NCO161	Equivalent Width of 1.61 μ m CO feature defined in Newton et al. 2015	0.1nm
NCO162	Equivalent Width of 1.62 μ m CO feature defined in Newton et al. 2015	0.1nm
NAL167A	Equivalent Width of 1.67 μ m Al-a feature defined in Newton et al. 2015	0.1nm
NAL167B	Equivalent Width of 1.67 μ m Al-b feature defined in Newton et al. 2015	0.1nm
NMG171	Equivalent Width of 1.71 μ m Mg feature defined in Newton et al. 2015	0.1nm
N15TEFF	Effective Temperature from Newton et al. 2015 calibration	K
N15RAD	Stellar Radius from Newton et al. 2015 calibration	solRad
N15LOGL	Logarithm of stellar luminosity from Newton et al. 2015 calibration	[solLum]
NOTES	Notes	...

^a Table 4 is published in its entirety in the electronic edition of The Astrophysical Journal Supplement

Gaidos et al. (2014) used the *V*-band spectroscopic calibration presented by M13a.

The comparison of our values to those from other works is shown in Figure 9, along with the median and scatter in each case. Our application of the M13a *K_s*-band [Fe/H] calibration shows good agreement with these other works, although we find systematically higher [Fe/H] for those stars with the highest [Fe/H] values compared to values reported in Rojas-Ayala et al. (2012) and (N14). This behavior may be a byproduct of the fea-

tures used in each case, whose sensitivity to [Fe/H] can saturate (as noted in N14). Particularly, the Na and Ca *K_s*-band features used in Rojas-Ayala et al. (2012), N14, and M14 are known to saturate as [Fe/H] approaches 0.5 dex.

The *H* and *J*-band calibrations are known to have larger scatter (M13a), and this is borne out in our comparisons of these measurements to other works. In both cases, the [Fe/H] we measure for stars with Solar [Fe/H] and higher is systematically 0.1–0.2 dex lower than that

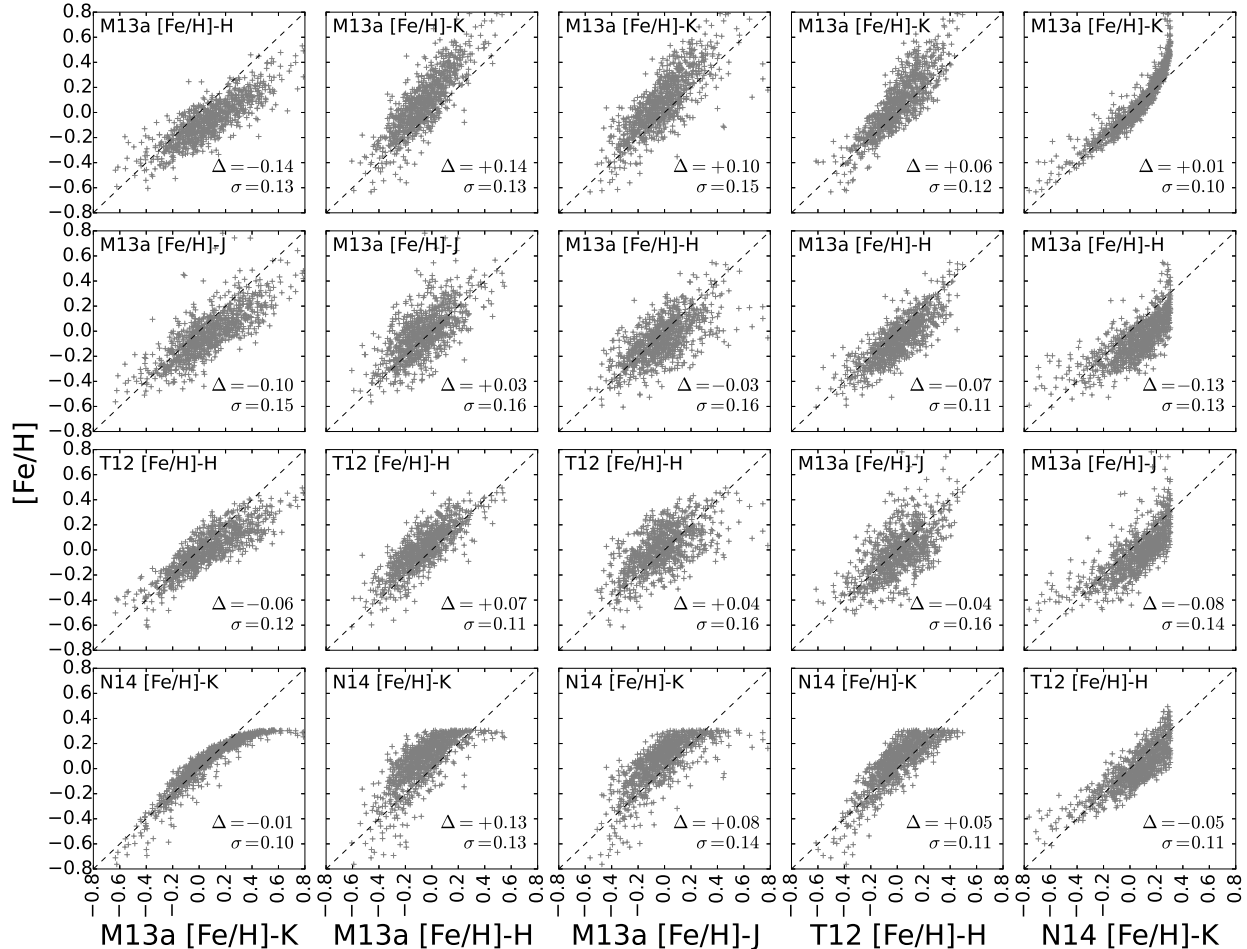


Figure 8. Comparisons between the different measures of $[\text{Fe}/\text{H}]$ included in our catalog (vertical axis, identified within each subplot), for all M dwarfs observed. The systematic offsets between the K_s -band measurements and the J, H -band measurements are evident. Each plot lists the median offset (Δ) and standard deviation (σ) of the differences, although these do not capture higher-order systematic differences.

reported in other works. This offset, which is not present for the K_s -band $[\text{Fe}/\text{H}]$ values, may result from structure remaining in the residuals of these calibrations as shown in e.g. Figure 5 of M13a.

There are several M dwarfs for which we measure later spectral type than M5, which also have $[\text{Fe}/\text{H}]$ reported in other works. For these stars, the N14 and Rojas-Ayala et al. (2012) calibrations appear to perform well compared to the M14 calibration, likely due to their common reliance on the K_s -band Na I feature.

Our application of the N14 $[\text{Fe}/\text{H}]$ calibration is consistent with the published $[\text{Fe}/\text{H}]$ measurements in their work, verifying our implementation. For targets in common with Rojas-Ayala et al. (2012), our $[\text{Fe}/\text{H}]$ measurements are systematically higher, consistent with the offset for later spectral types observed in Figure 18 of N14.

A similar catalog to the one presented here is that being developed for the CARMENES M dwarf exoplanet survey (Quirrenbach et al. 2014), for which an extensive optical spectroscopic survey has been carried out (Alonso-Floriano et al. 2015). There are 276 targets in the CARMENES catalog with coordinate matches in our catalog to within $5''$. We plot the respective measures

of composition and spectral type in Figure 10. As an indication of abundance, Alonso-Floriano et al. (2015) measure the $[\text{Fe}/\text{H}]$ -sensitive ζ parameter (based on TiO and CaH absorption in the optical, Lépine et al. 2007; Dhital et al. 2012). We find that ζ is weakly correlated with our measured $[\text{Fe}/\text{H}]$ (Kendall's $\tau = 0.25$, two-sided $p = 1.3 \times 10^{-8}$). This is unsurprising since ζ is a coarse indicator of abundance, which has been primarily used for discriminating between dwarfs and subdwarfs. For all targets in the overlap sample, our $[\text{Fe}/\text{H}]$ measurements and the ζ measurements of Alonso-Floriano et al. (2015) are both consistent with dwarf compositions. To measure spectral type, Alonso-Floriano et al. (2015) use a suite of spectral standard template matching and spectral index based techniques, and report spectral types to 0.5 subtypes. Our spectral type estimates broadly agree with those of Alonso-Floriano et al. (2015): our NIR M subtype measurements have a median offset of 0.37 with a residual standard deviation of 0.52, while our PMSU spectral types have a median offset of 0.12 subtypes and a residual standard deviation of 0.41. Alonso-Floriano et al. (2015) use PMSU standards for much of their reference set, so it is expected that the

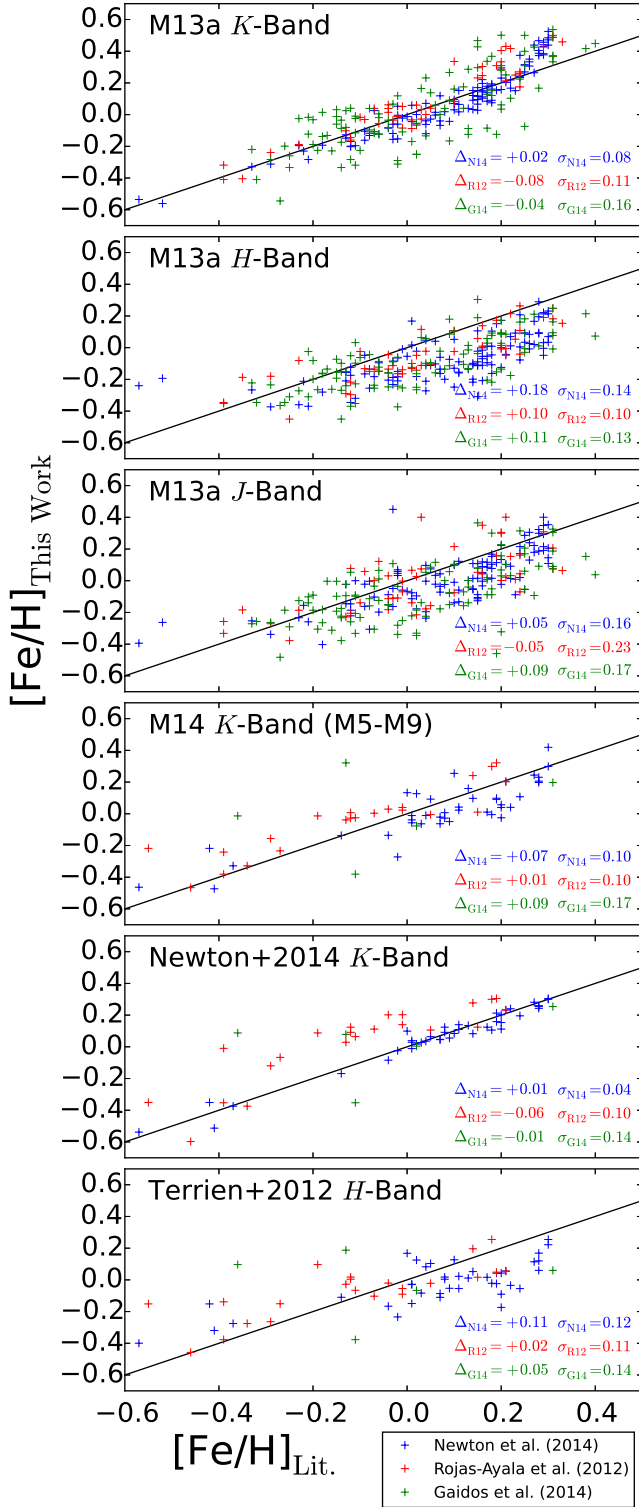


Figure 9. For stars in common with other recent surveys (Rojas-Ayala et al. 2012; Gaidos et al. 2014, N14), the comparison to $[\text{Fe}/\text{H}]$ values we measure. Each plot lists the median offset (Δ) and standard deviation (σ) of the differences, although these do not capture higher-order systematic differences.

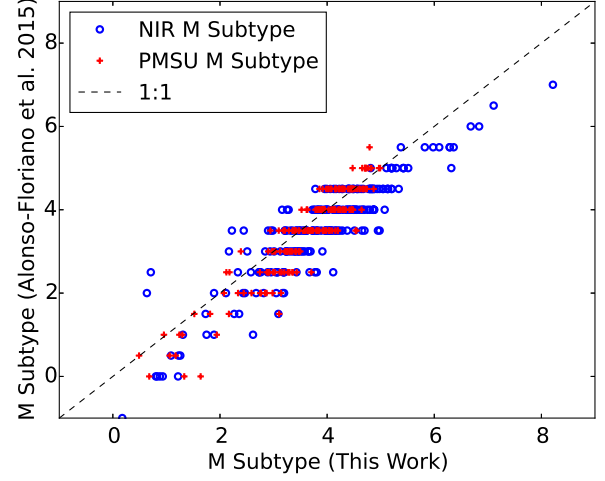


Figure 10. For stars in common the CARMENES target catalog (Alonzo-Floriano et al. 2015), the respective measures spectral type.

PMSU measurements should show better agreement.

5.3. Preferred Measure of $[\text{Fe}/\text{H}]$ for Early-Mid M Dwarfs

In light of the systematic offsets shown in Sections 5.1 and 5.2, it is useful to choose and justify a preferred measure of $[\text{Fe}/\text{H}]$ for M1-M5 dwarfs. We choose the K_s -band calibration of M13a for the following reasons:

- The breadth and number of calibrators exceeds those of other similar calibrations (T12, Rojas-Ayala et al. 2012; Newton et al. 2014).
- The better agreement between the K_s -band measurements and other literature measurements of the star (Section 5.2), which are themselves based on K_s -band features (Rojas-Ayala et al. 2012, , N14) and visible features (Gaidos et al. 2014).
- The stability against small RV shifts of the K_s -band measurements compared to those of the J and H -band of M13a.

5.4. $[\text{Fe}/\text{H}]$ and Stellar Kinematics

The stellar population of the Galaxy comprises multiple sub-populations with distinct kinematic, spatial, and compositional characteristics. These populations are often grouped into three components—the thin disk, the thick disk, and the Galactic halo (although the disk populations may be better-represented by a continuous distribution of populations than a bi-modal distribution, Bovy et al. 2012). Large scale surveys of FGK stars and luminous evolved stars have found rich information about the history and evolution of the Galaxy within the detailed abundances of these different populations (e.g. Bensby et al. 2003, 2014). Similar large-scale studies of M dwarfs (e.g. West et al. 2011; Bochanski et al. 2011) have also been carried out, and measurements of metallicity-sensitive band indices have enabled the identification and study of the oldest metal-poor M sub-dwarf populations (e.g. Bochanski et al. 2007). Refined metallicity measurement techniques are under development, and have demonstrated great potential for application with these large M dwarf catalogs (Dhital et al.

2010, 2012). Precise metallicity measurements of the M dwarfs in the solar neighborhood reveal correlations between composition and stellar kinematic and activity characteristics that are consistent with the increasing age and decreasing level of activity from the thin disk to the thick disk (Rojas-Ayala et al. 2012). These results suggest the promise of precise abundance measurements in these long-lived stars.

We explored whether the $[\text{Fe}/\text{H}]$ values in were consistent with the expected trends, as a check on our $[\text{Fe}/\text{H}]$ values and to probe for outliers and systematics. We calculated Galactocentric UVW motions for all of our targets with parallax measurements. Combining these parallaxes with proper motion values from LG11 and LSPM-N and RV measurements from the literature where available (or our RV measurements where literature RVs were unavailable), we have 283 targets with relatively precise UVW velocities (parallax error $< 10\%$, literature RV or measured RV error $< 10 \text{ km s}^{-1}$, no indications of binarity). These velocities are shown in the Toomre diagram in the left panel of Figure 11, along with rough demarcations of the thin disk, thick disk, and halo (Fuhrmann 2004). The Toomre diagram is effectively a projection of the rotational kinetic energy of each star relative to the local standard of rest, with stars of higher energies at increasing radii (Sandage & Fouts 1987). Consistent with expectations from galactic kinematics, those targets with the highest $[\text{Fe}/\text{H}]$ values are kinematically within the thin disk region, and targets with lower $[\text{Fe}/\text{H}]$ values are spread across the entire range of velocities. The right panel of Figure 11 shows the total Galactocentric velocity plotted against $\text{H}\alpha$ EW, a common activity indicator for M dwarfs (e.g. Reid et al. 1995; West et al. 2004; Walkowicz & Hawley 2009). The concentration of chromospherically active M dwarfs at low Galactocentric velocities, compared with the absence of active M dwarfs at higher velocities, suggests that we are indeed probing both the thick and thin disks, consistent with the chemical and kinematic properties of the M dwarfs in our catalog. The boundary between the thick and thin disk populations is not discrete (Ivezić et al. 2008), and there are indications that the compositional gradient between the thick and thin disks should be less than 1 dex (Bochanski et al. 2007), consistent with Figure 11.

The most significant outlier in these plots is CM Dra AB, a well-studied short-period eclipsing binary M dwarf system (e.g. Morales et al. 2009; Terrien et al. 2012a; Feiden & Chaboyer 2014). Constraints from the cooling age of a nearby co-moving white dwarf (Morales et al. 2009; Feiden & Chaboyer 2014) support the old age of this system, consistent with its high velocity, low $[\text{Fe}/\text{H}]$, and possible α -enrichment (Feiden & Chaboyer 2014; Terrien et al. 2015). That this system is chromospherically active at its old age is not surprising due to its short period (1.27 d) and the tidal interactions that have presumably taken place.

5.5. Metallicity and Stellar Colors

The infrared colors of M dwarfs have long been known to show sensitivity to stellar metallicity. This is in large part due to two primary sources of continuum opacity: H^- absorption and H_2O absorption. Lower-metallicity stars have higher H^- and H_2O absorption, leading to a loss of flux especially in the H -band

(Mould 1976; Leggett 1992). The effects of metallicity on infrared colors have been exploited by many authors to construct photometric metallicity calibrations (Johnson et al. 2012, M13a, N14), which are complementary (observationally cheaper but less precise) to the spectroscopic $[\text{Fe}/\text{H}]$ provided in this work.

As another check of the integrity of our catalog of metallicities, we show in Figure 12 the $(J - H, H - K_s)$ colors along with the $[\text{Fe}/\text{H}]$ values for each of our targets. We confirmed that our data show a tight relation between position in the $(J - H, H - K_s)$ -space and $[\text{Fe}/\text{H}]$, a connection established through examination of kinematically-defined populations in Leggett (1992). Also shown are the kinematic age boundaries derived in Leggett (1992), transformed to the 2MASS photometric system using the updated⁹ 2MASS color transformations (Carpenter 2001).

5.6. Planet Hosts

Stellar composition is of fundamental importance in studies of exoplanets. The properties of observational relationships relating to composition, including the giant planet-metallicity (Fischer & Valenti 2005) and the planet mass-metallicity (Ghezzi et al. 2010) correlations, provide unique insight into the environments and mechanisms of planet formation. Moreover, reliable planet host star compositions are necessary in order to apply empirical relationships to derive the stellar luminosities and temperatures (Boyajian et al. 2012; Muirhead et al. 2014; Mann et al. 2015), and hence the location of the Habitable Zone (e.g. Muirhead et al. 2012a, M13b).

This breadth of impact motivates the empirical and theoretical efforts to define an M dwarf metallicity scale. Multiple groups have already shown that the giant planet-metallicity correlation extends to the M dwarf regime (Johnson & Apps 2009; Neves et al. 2013b). A well-calibrated and precise metallicity scale is crucial for these and future studies of M dwarf planet populations. The metallicity values in this catalog are derived from the most precise and well-calibrated scales available for M dwarfs, and it is valuable to compare our results with those of previous studies for planet-hosting M dwarfs.

Our catalog includes 16 M dwarfs that are known to be planet hosts, and in Table 5 we show our measured $[\text{Fe}/\text{H}]$, $[\text{M}/\text{H}]$, and $\text{H}_2\text{O-K2}$ based spectral types. Generally, we measure metallicities consistent with those of previous NIR spectroscopic studies. In many cases our $[\text{Fe}/\text{H}]$ measurements are substantially different from previous photometric estimates, which is expected as those calibrations are inherently less precise and use fewer calibrators than the relations we employed.

6. CONCLUSION

We have presented NIR spectra and spectroscopic parameters for 886 nearby M dwarfs. This catalog represents the largest such compilation of M dwarf abundances, T_{eff} -sensitive indices, and NIR spectra yet published, and includes:

- $[\text{Fe}/\text{H}]$ and $[\text{M}/\text{H}]$ measurements (uncertainty ~ 0.1 dex) for M1-M5 dwarfs using J , H , and K_s -band features, derived from multiple published calibrations.

⁹ <http://www.astro.caltech.edu/~jmc/2mass/v3/transformations/>

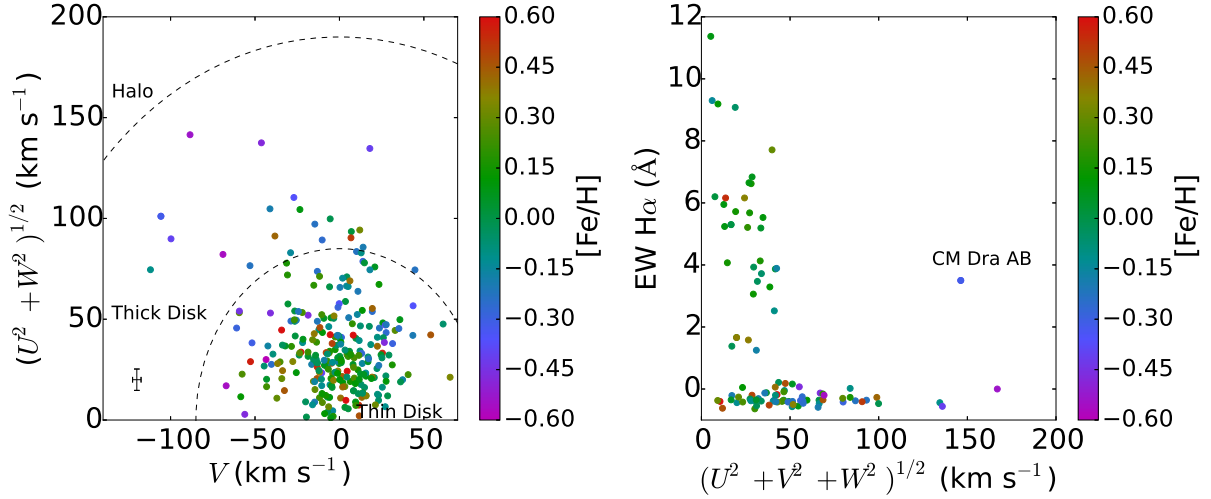


Figure 11. (*Left*): The Toomre diagram for survey targets with measured parallax. The halo, thick disk, and thin disk regions are denoted. There are no metal-rich M dwarfs with thick-disk kinematics in our sample, consistent with expectations. A typical error bar is plotted in the lower left. (*Right*): The total Galactocentric velocity versus H α EW (positive indicates emission and therefore more chromospheric activity). Indicators of both [Fe/H] and activity (H α) suggest that our catalog probes both the thick and thin disks.

Table 5
Measured parameters for known planet hosts

Name	B05 ^a [Fe/H]	JA09 ^a [Fe/H]	W09 ^a [Fe/H]	SL10 ^a [Fe/H]	RA10 ^a [Fe/H]	RA12 ^a [Fe/H]	N12 ^a [Fe/H]	T12 ^a [Fe/H]	N14 ^a [Fe/H]	other	[Fe/H] ^b	This Work [M/H] ^c	NIR SpT
GJ 1214	...	+0.03	...	+0.28	+0.39	+0.20	+0.03	...	+0.05	...	+0.40	+0.27	M4.5
HIP 57050	-0.02	+0.32	+0.07	...	+0.12	+0.04	...	+0.05	+0.04	-0.03	M4.0
GJ 876	+0.03	+0.37	+0.02	+0.23	+0.43	+0.19	+0.14	+0.11	+0.14	...	+0.31	+0.19	M3.5
GJ 317	+0.22	+0.31	+0.22	...	+0.43	+0.30	M3.5
GJ 581	-0.25	-0.10	-0.10	-0.22	-0.02	-0.10	-0.18	-0.09	-0.20	...	-0.02	-0.03	M3.0
GJ 179	...	+0.30	+0.02	+0.20	...	+0.23	+0.14	+0.18	+0.12	...	+0.25	+0.12	M3.0
HIP 79431	+0.16	+0.52	...	+0.35	+0.60	+0.46	...	+0.50	+0.78 ^d	+0.55	M2.5
GJ 436	-0.03	+0.25	-0.05	+0.10	+0.00	+0.05	+0.01	+0.02	-0.03	...	+0.00	-0.03	M2.5
GJ 849	+0.14	+0.58	+0.20	+0.41	+0.49	+0.31	+0.24	+0.22	+0.22	...	+0.50	+0.33	M2.5
GJ 3470	+0.20 ^e	+0.27	+0.15	M2.0
GJ 15A	-0.36 ^f	-0.28	-0.17	M2.0
GJ 649	-0.18	+0.04	-0.13	-0.03	+0.14	-0.04	...	-0.05	+0.04	-0.01	M1.5
GJ 433	-0.13	...	-0.17	...	-0.03	-0.06	M1.5
Kepler-138	-0.18 ^g	-0.21	-0.16	M1.0
WASP-80	-0.14 ^h	+0.13	+0.07	M0.5
WASP-43	+0.01 ⁱ	+0.40	+0.28	M0.5

^a B05:Bonfils et al. (2005), JA09:Johnson & Apps (2009), W09:Woolf et al. (2009), SL10:Schlaufman & Laughlin (2010), RA10:Rojas-Ayala et al. (2010), RA12:Rojas-Ayala et al. (2012), N12:Neves et al. (2012), T12:Terrien et al. (2012b), N14:Neves et al. (2014)

^b Uncertainties in [Fe/H] are approximately 0.11 dex

^c Uncertainties in [M/H] are approximately 0.10 dex

^d This star is well outside the calibrated range ($-1.04 < [\text{Fe}/\text{H}] < +0.56$) of [Fe/H].

^e (Demory et al. 2013)

^f (Neves et al. 2013a)

^g [M/H] value from Muirhead et al. (2012a)

^h (Triaud et al. 2013)

ⁱ (Chen et al. 2014)

- [Fe/H] with similar uncertainties derived from K_s -band features for M5-M8 dwarfs.
- Measurements of J, H, K_s -band H₂O-based and other indices which are known to track T_{eff} .
- Measurements of strengths of the 820 nm Na I doublet and the 860nm Ca II triplet, which are sensitive to activity and surface gravity.
- Stellar photometry and astrometry from the literature.

- RVs (uncertainty $\sim 10 \text{ km s}^{-1}$).

We performed cross-checks among the different [Fe/H] calibrations within our catalog and in the literature. We uncovered some systematic issues with the implementations of the J and H -band calibrations, which led us to select the K_s -band calibration of M13a as the preferred measure of [Fe/H] for M1-M5 dwarfs where multiple calibrations exist. Using this [Fe/H], we confirmed the expected trends with Galactocentric velocity activity levels, and stellar colors. We also provide updated abundances measurements for many of the known M dwarf exoplanet

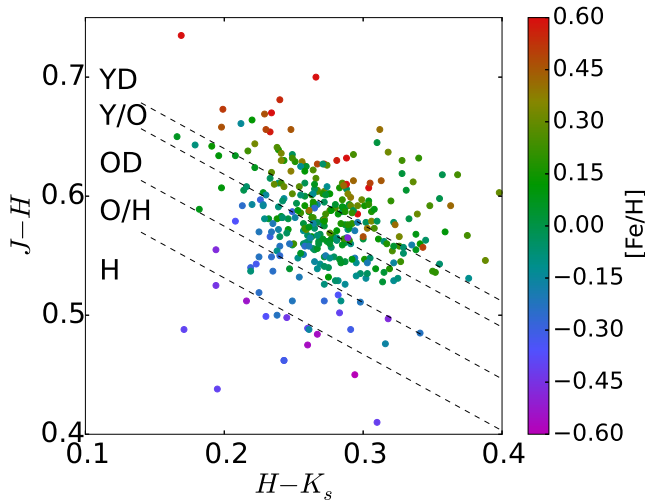


Figure 12. A NIR color-color diagram for survey targets with high-quality (AAA) 2MASS photometry and no indications of multiplicity. The position in $(J - H, H - K_s)$ space is well-correlated with metallicity, as noted in (Leggett 1992).

hosts.

The original motivation for this survey was to support upcoming planet surveys targeting M dwarfs, including ground-based RV surveys (Mahadevan et al. 2014; Quirrenbach et al. 2014; Thibault et al. 2012; Kotani et al. 2014) and space-based transit surveys (Rauer et al. 2014; Ricker et al. 2015), to enable both survey target planning and rapid interpretation of results (e.g. whether a planet is in the Habitable Zone of its host star). This catalog will also be useful for other studies of the nearby M dwarfs, and has already proven its value in this context. Data from this catalog enabled insight into the tension between observations and model predictions for the eclipsing binary CM Dra (Terrien et al. 2012a), supported the first confirmation of the low-mass members of the Coma Berenices cluster (Terrien et al. 2014), and were used to demonstrate the use of new gravity and activity-sensitive spectral indices (Terrien et al. 2015). This collection of M dwarf spectra provide a rich dataset on which to build even better calibrations, or to discover new useful features.

It is our hope that this dataset, complementing other similar recent works (e.g. Rojas-Ayala et al. 2012; Lépine et al. 2013; Newton et al. 2014; Gaidos et al. 2014; Alonso-Floriano et al. 2015), will facilitate the work of other groups working to understand the nearby M dwarfs, and to further our understanding of these most common stars and their planets.

We thank Dr. Kevin Luhman for obtaining observations of a subset of these targets. We also thank the referee, Dr. Andrew Mann, for a thorough and insightful review.

This work was partially supported by funding from the Center for Exoplanets and Habitable Worlds. The Center for Exoplanets and Habitable Worlds is supported by the Pennsylvania State University, the Eberly College of Science, and the Pennsylvania Space Grant Consortium. This work was also partially supported by the Penn State Astrobiology Research Center and the National Aeronautics and Space Administration (NASA) Astrobiology In-

stitute. We acknowledge support from NSF grants AST 1006676, AST 1126413, and AST 1310885 in our pursuit of precision radial velocities in the NIR. This research has made use of the SIMBAD database, operated at CDS, Strasbourg, France. This publication makes use of data products from the Two Micron All Sky Survey, which is a joint project of the University of Massachusetts and the Infrared Processing and Analysis Center/California Institute of Technology, funded by the National Aeronautics and Space Administration and the National Science Foundation.

The authors wish to recognize and acknowledge the very significant cultural role and reverence that the summit of Mauna Kea has always had within the indigenous Hawaiian community. We are most fortunate to have the opportunity to conduct observations from this mountain.

REFERENCES

- Allard, F., Homeier, D., & Freytag, B. 2012, *Philosophical Transactions of the Royal Society A: Mathematical, Physical and Engineering Sciences*, 370, 2765
- Alonso-Floriano, F. J., Morales, J. C., Caballero, J. A., et al. 2015, *Astronomy and Astrophysics*, doi:10.1051/0004-6361/201525803
- Anglada-Escudé, G., Boss, A. P., Weinberger, A. J., et al. 2012, *The Astrophysical Journal*, 746, 37
- Ballard, S., Charbonneau, D., Fressin, F., et al. 2013, *The Astrophysical Journal*, 773, 98
- Baraffe, I., Chabrier, G., Allard, F., & Hauschildt, P. H. 1998, *Astronomy and Astrophysics*, 337, 403
- Barnes, J. R., Jenkins, J. S., Jones, H. R. A., et al. 2014, *Monthly Notices of the Royal Astronomical Society*, 439, 3094
- Bensby, T., Feltzing, S., & Lundström, I. 2003, *Astronomy and Astrophysics*, 410, 527
- Bensby, T., Feltzing, S., & Oey, M. S. 2014, *Astronomy and Astrophysics*, 562, A71
- Bochanski, J. J., Hawley, S. L., Covey, K. R., et al. 2010, *The Astronomical Journal*, 139, 2679
- Bochanski, J. J., Hawley, S. L., & West, A. A. 2011, *The Astronomical Journal*, 141, 98
- Bochanski, J. J., Munn, J. A., Hawley, S. L., et al. 2007, *The Astronomical Journal*, 134, 2418
- Bonfils, X., Delfosse, X., Udry, S., et al. 2005, *Astronomy and Astrophysics*, 442, 635
- Borucki, W. J., Koch, D., Basri, G., et al. 2010, *Science*, 327, 977
- Bovy, J., Rix, H.-W., & Hogg, D. W. 2012, *The Astrophysical Journal*, 751, 131
- Boyajian, T. S., von Braun, K., van Belle, G., et al. 2012, *The Astrophysical Journal*, 757, 112
- Carpenter, J. M. 2001, *The Astronomical Journal*, 121, 2851
- Carter, J. A., Fabrycky, D. C., Ragozzine, D., et al. 2011, *Science*, 331, 562
- Casagrande, L., Schönrich, R., Asplund, M., et al. 2011, *Astronomy and Astrophysics*, 530, A138
- Chabrier, G., Baraffe, I., Allard, F., & Hauschildt, P. 2000, *The Astrophysical Journal*, 542, 464
- Chen, G., van Boekel, R., Wang, H., et al. 2014, *Astronomy and Astrophysics*, 563, A40
- Chubak, C., Marcy, G., Fischer, D. A., et al. 2012, eprint arXiv:1207.6212
- Covey, K. R., Lada, C. J., Román-Zúñiga, C., et al. 2010, *The Astrophysical Journal*, 722, 971
- Cushing, M. C., Rayner, J. T., & Vacca, W. D. 2005, *The Astrophysical Journal*, 623, 1115
- Cushing, M. C., Vacca, W. D., & Rayner, J. T. 2004, *The Publications of the Astronomical Society of the Pacific*, 116, 362
- Delfosse, X., Forveille, T., Ségransan, D., et al. 2000, *Astronomy and Astrophysics*, 364, 217
- Demory, B. O., Ségransan, D., Forveille, T., et al. 2009, *Astronomy and Astrophysics*, 505, 205
- Demory, B.-O., Torres, G., Neves, V., et al. 2013, *The Astrophysical Journal*, 768, 154

- Deshpande, R., Blake, C. H., Bender, C. F., et al. 2013, *The Astronomical Journal*, 146, 156
- Dhital, S., West, A. A., Stassun, K. G., & Bochanski, J. J. 2010, *The Astronomical Journal*, 139, 2566
- Dhital, S., West, A. A., Stassun, K. G., et al. 2012, *The Astronomical Journal*, 143, 67
- Dittmann, J. A., Irwin, J. M., Charbonneau, D., & Berta-Thompson, Z. K. 2014, *The Astrophysical Journal*, 784, 156
- Dotter, A., Chaboyer, B., Ferguson, J. W., et al. 2007, *The Astrophysical Journal*, 666, 403
- Dressing, C. D., & Charbonneau, D. 2015, *The Astrophysical Journal*, 807, 45
- Feiden, G. A., & Chaboyer, B. 2012, *The Astrophysical Journal*, 757, 42
- . 2014, *Astronomy and Astrophysics*, 571, A70
- Fischer, D. A., & Valenti, J. 2005, *The Astrophysical Journal*, 622, 1102
- Frith, J., Pinfield, D. J., Jones, H. R. A., et al. 2013, *Monthly Notices of the Royal Astronomical Society*, 435, 2161
- Fuhrmann, K. 2004, *Astronomische Nachrichten*, 325, 3
- Gaidos, E., Mann, A. W., Lépine, S., et al. 2014, *Monthly Notices of the Royal Astronomical Society*, 443, 2561
- Galvez-Ortiz, M. C., Kuznetsov, M., Clarke, J. R. A., et al. 2014, *Monthly Notices of the Royal Astronomical Society*, 439, 3890
- Gatewood, G. 2008, *The Astronomical Journal*, 136, 452
- Ghezzi, L., Cunha, K., Smith, V. V., et al. 2010, *The Astrophysical Journal*, 720, 1290
- Gizis, J. E. 1997, *Astronomical Journal* v.113, 113, 806
- Gizis, J. E., Reid, I. N., & Hawley, S. L. 2002, *The Astronomical Journal*, 123, 3356
- Gould, A., & Chaname, J. 2004, *The Astrophysical Journal Supplement Series*, 150, 455
- Gustafsson, B. 1989, IN: Annual review of astronomy and astrophysics. Volume 27 (A90-29983 12-90). Palo Alto, 27, 701
- Harrington, R. S., Dahn, C. C., Kallarakal, V. V., et al. 1993, *The Astronomical Journal*, 105, 1571
- Hawley, S. L., Gizis, J. E., & Reid, I. N. 1996, *The Astrophysical Journal*, 112, 2799
- Hejazi, N., Robertis, M. M. D., & Dawson, P. C. 2015, *The Astronomical Journal*, 149, 140
- Henry, T. J., Jao, W.-C., Subasavage, J. P., et al. 2006, *The Astronomical Journal*, 132, 2360
- Ivezić, Ž., Sesar, B., Jurić, M., et al. 2008, *The Astrophysical Journal*, 684, 287
- Janson, M., Bergfors, C., Brandner, W., et al. 2014, *The Astrophysical Journal*, 789, 102
- Jao, W.-C., Henry, T. J., Subasavage, J. P., et al. 2005, *The Astronomical Journal*, 129, 1954
- . 2011, *The Astronomical Journal*, 141, 117
- Johnson, J. A., & Apps, K. 2009, *The Astrophysical Journal*, 699, 933
- Johnson, J. A., Gazak, J. Z., Apps, K., et al. 2012, *The Astronomical Journal*, 143, 111
- Kafka, S., & Honeycutt, R. K. 2006, *The Astronomical Journal*, 132, 1517
- Kasting, J. 1993, *Icarus*, 101, 108
- Kopparapu, R. k., Ramirez, R. M., SchottelKotte, J., et al. 2014, *The Astrophysical Journal*, 787, L29
- Kopparapu, R. k., Ramirez, R., Kasting, J. F., et al. 2013, *The Astrophysical Journal*, 765, 131
- Kotani, T., Tamura, M., Suto, H., et al. 2014, in *Astronomical Telescopes and Instrumentation: Synergies Between Ground and Space*, ed. S. K. Ramsay, I. S. McLean, & H. Takami (SPIE), 914714
- Laughlin, G., Bodenheimer, P., & Adams, F. C. 2004, *The Astrophysical Journal*, 612, L73
- Leggett, S. K. 1992, *Astrophysical Journal Supplement Series*, 82, 351
- Lépine, S., & Gaidos, E. 2011, *The Astronomical Journal*, 142, 138
- Lépine, S., Hilton, E. J., Mann, A. W., et al. 2013, *The Astronomical Journal*, 145, 102
- Lépine, S., Rich, R. M., & Shara, M. M. 2007, *The Astrophysical Journal*, 669, 1235
- Lépine, S., & Shara, M. M. 2005, *The Astronomical Journal*, 129, 1483
- Lépine, S., Thorstensen, J. R., Shara, M. M., & Rich, R. M. 2009, *The Astronomical Journal*, 137, 4109
- Lopez-Morales, M. 2007, *The Astrophysical Journal*, 660, 732
- Mahadevan, S., Ramsey, L., Bender, C., et al. 2012, *Ground-based and Airborne Instrumentation for Astronomy IV*, 8446, 84461S
- Mahadevan, S., Ramsey, L. W., Terrien, R., et al. 2014, in *Astronomical Telescopes and Instrumentation: Synergies Between Ground and Space*, ed. S. K. Ramsay, I. S. McLean, & H. Takami (SPIE), 91471G
- Maldonado, J., Affer, L., Micela, G., et al. 2015, eprint arXiv:1503.03010
- Mann, A. W., Brewer, J. M., Gaidos, E., Lépine, S., & Hilton, E. J. 2013a, *The Astronomical Journal*, 145, 52
- Mann, A. W., Deacon, N. R., Gaidos, E., et al. 2014, *The Astronomical Journal*, 147, 160
- Mann, A. W., Feiden, G. A., Gaidos, E., Boyajian, T., & von Braun, K. 2015, *The Astrophysical Journal*, 804, 64
- Mann, A. W., Gaidos, E., & Ansdell, M. 2013b, *The Astrophysical Journal*, 779, 188
- Martín, E. L., Phan-Bao, N., Bessell, M., et al. 2010, *Astronomy and Astrophysics*, 517, A53
- Monet, D. G., Dahn, C. C., Vrba, F. J., et al. 1992, *The Astronomical Journal*, 103, 638
- Morales, J. C., Ribas, I., Jordi, C., et al. 2009, *The Astrophysical Journal*, 691, 1400
- Mould, J. R. 1976, *Astronomy and Astrophysics*, 48, 443
- Muirhead, P. S., Hamren, K., Schlawin, E., et al. 2012a, *The Astrophysical Journal*, 750, L37
- Muirhead, P. S., Johnson, J. A., Apps, K., et al. 2012b, *The Astrophysical Journal*, 747, 144
- Muirhead, P. S., Vanderburg, A., Shporer, A., et al. 2013, *The Astrophysical Journal*, 767, 111
- Muirhead, P. S., Becker, J., Feiden, G. A., et al. 2014, *The Astrophysical Journal Supplement Series*, 213, 5
- Neves, V., Bonfils, X., Santos, N. C., et al. 2013a, *Astronomy and Astrophysics*, 551, A36
- . 2013b, *Astronomy and Astrophysics*, 551, A36
- . 2014, *Astronomy and Astrophysics*, 568, A121
- . 2012, *Astronomy and Astrophysics*, 538, 25
- Newton, E. R., Charbonneau, D., Irwin, J., et al. 2014, *The Astronomical Journal*, 147, 20
- Newton, E. R., Charbonneau, D., Irwin, J., & Mann, A. W. 2015, *The Astrophysical Journal*, 800, 85
- Nutzman, P., & Charbonneau, D. 2008, *Publications of the Astronomical Society of the Pacific*, 120, 317
- Önehag, A., Heiter, U., Gustafsson, B., et al. 2012, *Astronomy and Astrophysics*, 542, A33
- Park, C., Jaffe, D. T., Yuk, I.-S., et al. 2014, in *Astronomical Telescopes and Instrumentation: Synergies Between Ground and Space*, ed. S. K. Ramsay, I. S. McLean, & H. Takami (SPIE), 91471D
- Pineda, J. S., Bottom, M., & Johnson, J. A. 2013, *The Astrophysical Journal*, 767, 28
- Pravdo, S. H., Shaklan, S. B., & Lloyd, J. 2005, *The Astrophysical Journal*, 630, 528
- Quirrenbach, A., Amado, P. J., Seifert, W., et al. 2012, *Ground-based and Airborne Instrumentation for Astronomy IV*, 8446, 84460R
- Quirrenbach, A., Amado, P. J., Caballero, J. A., et al. 2014, in *SPIE Astronomical Telescopes + Instrumentation*, ed. S. K. Ramsay, I. S. McLean, & H. Takami (SPIE), 91471F
- Rajpurohit, A. S., Reyle, C., Allard, F., et al. 2013, *Astronomy and Astrophysics*, 556, A15
- Rauer, H., Catala, C., Aerts, C., et al. 2014, *Experimental Astronomy*, 38, 249
- Rayner, J. T., Cushing, M. C., & Vacca, W. D. 2009, *The Astrophysical Journal Supplement*, 185, 289
- Rayner, J. T., Toomey, D. W., Onaka, P. M., et al. 2003, *The Publications of the Astronomical Society of the Pacific*, 115, 362
- Reid, I. N., Gizis, J. E., & Hawley, S. L. 2002, *The Astronomical Journal*, 124, 2721
- Reid, I. N., Hawley, S. L., & Gizis, J. E. 1995, *The Astronomical Journal*, 110, 1838
- Reiners, A., Joshi, N., & Goldman, B. 2012, *The Astronomical Journal*, 143, 93

- Riaz, B., Gizis, J. E., & Harvin, J. 2006, *The Astronomical Journal*, 132, 866
- Ricker, G. R., Winn, J. N., Vanderspek, R., et al. 2015, *Journal of Astronomical Telescopes, Instruments, and Systems*, 1, 014003
- Riedel, A. R., Subasavage, J. P., Finch, C. T., et al. 2010, *The Astronomical Journal*, 140, 897
- Riedel, A. R., Finch, C. T., Henry, T. J., et al. 2014, *The Astronomical Journal*, 147, 85
- Roeser, S., Demleitner, M., & Schilbach, E. 2010, *The Astronomical Journal*, 139, 2440
- Rojas-Ayala, B., Covey, K. R., Muirhead, P. S., & Lloyd, J. P. 2010, *The Astrophysical Journal*, 720, L113
- . 2012, *The Astrophysical Journal*, 748, 93
- Sandage, A., & Fouts, G. 1987, *The Astronomical Journal*, 93, 592
- Schlaufman, K. C., & Laughlin, G. 2010, *Astronomy and Astrophysics*, 519, 105
- Schlieder, J. E., Lépine, S., Rice, E., et al. 2012, *The Astronomical Journal*, 143, 114
- Shkolnik, E. L., Anglada-Escudé, G., Liu, M. C., et al. 2012, *The Astrophysical Journal*, 758, 56
- Skrutskie, M. F., Cutri, R. M., Stiening, R., et al. 2006, *The Astronomical Journal*, 131, 1163
- Spada, F., Demarque, P., Kim, Y. C., & Sills, A. 2013, *The Astrophysical Journal*, 776, 87
- Terrien, R. C., Fleming, S. W., Mahadevan, S., et al. 2012a, *The Astrophysical Journal*, 760, L9
- Terrien, R. C., Mahadevan, S., Bender, C. F., et al. 2012b, *The Astrophysical Journal Letters*, 747, L38
- Terrien, R. C., Mahadevan, S., Bender, C. F., Deshpande, R., & Robertson, P. 2015, *The Astrophysical Journal*, 802, L10
- Terrien, R. C., Mahadevan, S., Deshpande, R., et al. 2014, *The Astrophysical Journal*, 782, 61
- Thibault, S., Rabou, P., Donati, J.-F., et al. 2012, *Ground-based and Airborne Instrumentation for Astronomy IV*, 8446, 844630
- Torres, G. 2013, *Astronomische Nachrichten*, 334, 4
- Triaud, A. H. M. J., Anderson, D. R., Collier Cameron, A., et al. 2013, *Astronomy and Astrophysics*, 551, A80
- Trumpler, R. J. 1938, *Lick Observatory Bulletin*, 18, 167
- Vacca, W. D., Cushing, M. C., & Rayner, J. T. 2003, *Publications of the Astronomical Society of the Pacific*, 115, 389
- van Altena, W. F., Lee, J. T., & Hoffleit, D. 1995, *VizieR Online Data Catalog*, 1174, 0
- van Leeuwen, F. 2007, *Astronomy and Astrophysics*, 474, 653
- Walkowicz, L. M., & Hawley, S. L. 2009, *The Astronomical Journal*, 137, 3297
- West, A. A., Hawley, S. L., Walkowicz, L. M., et al. 2004, *The Astronomical Journal*, 128, 426
- West, A. A., Morgan, D. P., Bochanski, J. J., et al. 2011, *The Astronomical Journal*, 141, 97
- Wilking, B. A., Greene, T. P., & Meyer, M. R. 1999, *AJ*, 117, 469
- Winters, J. G., Henry, T. J., Jao, W.-C., et al. 2011, *The Astronomical Journal*, 141, 21
- Wolf, V. M., Lépine, S., & Wallerstein, G. 2009, *Publications of the Astronomical Society of the Pacific*, 121, 117
- Wolf, V. M., & Wallerstein, G. 2005, *Monthly Notices of the Royal Astronomical Society*, 356, 963
- . 2006, *The Publications of the Astronomical Society of the Pacific*, 118, 218
- Zacharias, N., Finch, C. T., Girard, T. M., et al. 2013, *The Astronomical Journal*, 145, 44